THE PENNSYLVANIA STATE UNIVERSITY
SCHREYER HONORS COLLEGE

DEPARTMENT OF MECHANICAL AND NUCLEAR ENGINEERING

DEVELOPMENT AND TESTING OF A WASTE HEAT RECOVERY SYSTEM THROUGH THERMOELECTRIC GENERATORS (TEG)

SHIVEN RAJENDRA PATEL
FALL 2017

A thesis
submitted in partial fulfillment
of the requirements
for a baccalaureate degree
in Mechanical Engineering
with honors in Mechanical Engineering

Reviewed and approved* by the following:

Dr. Sean Brennan
Professor of Mechanical and Nuclear Engineering
Honors Advisor

Dr. Alexander Rattner
Assistant Professor of Mechanical and Nuclear Engineering
Thesis Supervisor

* Signatures are on file in the Schreyer Honors College.

ABSTRACT

One of the challenges limiting the implementation of thermoelectric material in thermal systems, in which significant heat is lost to the environment, is its limited power generation efficiency. A team of researchers led by Penn State are designing, building and optimizing a waste heat absorption facility through Thermoelectric Generators (TEGs) modules to understand the optimal conditions for TEG performance. This thesis focuses on the design of an HX Enclosure to enhance heat transfer from the heat source to the TEGs and the testing of the waste heat recovery system. The system is built as a TEG/Oil Loop, in which inlet air and cold oil (Paratherm NF) flow through the designed HX Enclosure. The design of the enclosure was done through SolidWorks modeling, and the testing of the system required a variety of thermocouple sensors to monitor relevant temperatures and flow rates.

This thesis presents results from an initial theoretical model, calculated through modeling the system's thermal resistance network, and results from tests conducted on the system at various inlet temperature and flow rate conditions to understand the effects varying these inputs have on TEG performance. These performance tests will allow engineers to understand the viability of assumptions made in the theoretical model. The work in this thesis analyzes the significance of these test results and provides insight into understanding the optimal conditions for the TEG's performance.

TABLE OF CONTENTS

LIST OF FIGURES

LIST OF TABLES

ACKNOWLEDGEMENTS

First, I would like to thank my thesis advisor, Dr. Alexander Rattner. Dr. Rattner consistently went way beyond his duties as my thesis advisor. He made time during his busy schedule to not only guide me through all questions and concerns regarding my thesis topic, but also provide physical support in the setup of our experimental system. I cannot emphasize my gratitude towards Dr. Rattner for being an outstanding professor, and advisor, during my time at Penn State. Dr. Rattner was involved throughout each step of my research, experimentation and analysis. It is safe to say that Dr. Rattner was instrumental in the successful completion of my thesis, as I navigated through a busy final semester towards graduation from Penn State.

I would also like to thank Shahzaib Abbasi for his constant support throughout my research and experimentation. Shahzaib was integral to my completion of this thesis and assisted me throughout designing the HX enclosure, developing the thermal resistance network calculations, and running the experiments in our laboratory. Shahzaib was extremely patient and a great mentor and I am very grateful for his assistance in the completion of this thesis.

Finally, I would like to thank Dr. Sean Brennan, my honors advisor. Dr. Brennan has provided great support during my time at Penn State, both academically and professionally. Dr. Brennan has helped me navigate through tough academic situations, despite his extremely busy schedule. I am glad to have had Dr. Brennan as my advisor during my time at Penn State.

Chapter 1

Introduction

This thesis focuses on the application of thermoelectric generators (TEGs) coupled with a heat sink enclosure as a waste heat recovery system. There are strong economic opportunities to improve fuel economy by improving the efficiency of internal combustion engines (ICEs) and heating and cooling (HVAC) systems. Due to the inefficiency of these widely-deployed systems, and large-scale saving opportunities, the heat sink-TEG system is being designed and tested to determine the heat sink enclosure design and experimental efficiency results of the system.

1.1 Motivation

There are several sources of motivation for this work. The first is that HVAC and ICE systems are used every day, but do not operate near optimal thermal efficiency. The Department of Energy has stated the desire to improve the efficiency of internal combustion engines from 42 percent to 50 percent (a 20 percent improvement) [1]. Economically, 1 percent and 5 percent fuel savings for personal trucks results in $5.0B and $25.0B estimated fuel savings over 1 year, respectively [2]. Extrapolating these fuel savings to other commercial vehicles has garnered interest from many automotive OEMs.

This project seeks to quantify the electrical output of TEGs within a thermal system powered by a heat fan. An innovative heat sink enclosure and executing a characterization matrix, testing several

variables, is leading the author to experimentally determining the efficiency of TEGs. The result of this thesis is meant to validate the TEG approach as a feasible waste heat recovery system. Scaling this test to larger systems can realize the Department of Energy's desire to improve automotive thermal efficiencies.

1.2 Research Objective

The research objectives of this project are to develop a heat sink enclosure to facilitate the heat transfer of "waste heat" from the heat blower to the TEGs. To motivate TEG implementation, approximately 60% of the energy consumed globally is wasted in the form of low-grade heat. In automobiles, the ICE does not efficiently convert thermal energy into mechanical energy, losing much of the energy as dissipated heat in the coolant and exhaust. The HVAC and ICE systems are characterized by large temperature differentials, offering the ability to implement TEG technology, converting the temperature gradient into electrical output. The main research objectives of this thesis are to: research, prototype and manufacture the optimal HX enclosure design, develop a thermal resistance network and performance matrix, and perform analysis of experimental test results for optimal TEG conditions.

During the design phase of the project, the enclosure must go through several iterations to be customized to the TEG/heat loop system and designed for minimal dissipated heat loss. The heat blower funnels heat into a large cylindrical tube, which serves as the design constraint to ensure negligible heat loss to the surroundings. Additionally, the enclosure assembly must be designed giving the constraints of the heat sinks attached inside the enclosure, to enhance heat flow. The

design of the HX enclosure with respect to the TEG, water block, and heat loop is a crucial step in this project.

Modeling the thermal resistance network of the TEG/HX system is another research objective. While the resistance due to convection, conduction and interface resistance are identified, the specific system's resistances must be calculated. Identifying the relevant system parameters, such as heat transfer coefficients and overall thermal resistance, allows the team to explore varying inputs in efforts to attain a maximum electrical output from the TEGs. Another objective is to develop a characterization matrix, which allows the author to variate several system parameters, such as flow rates, temperature of the air and system oil, type of oil, etc. The placement of the TEGs with respect to the heat absorber, heat sink and HX enclosure is a constant while simulating the test matrix. Attaching multiple TEGs on stacked wall faces, as done in this thesis experimentation, strongly affects the unit area generation [3]. The results of these tests will allow the team to determine the optimal conditions for TEG output and apply the findings from experimentation to real waste heat recovery systems.

1.3 Project Background

In the 1820s, Thomas Seebeck developed a circuit with junctions at different temperatures. Through testing with a compass magnet, Seebeck determined a "Thermoelectric Force" exists, which states that a temperature gradient produces an electrical potential (Voltage), which can drive an electric current in a circuit [4]. Furthermore, the voltage produced is proportional to the temperature gradient between the two junctions. This concept has seen been expanded through

thermoelectric generators. TEGs utilize the Seebeck effect with N-type and P-type semiconductor materials connected electrically in series, but thermally in parallel [5]. Below is a graphic visualizing the Seebeck Effect phenomena, with an equivalent thermoelectric circuit in place, highlighting in Figure 1b that the amount of electric power produced is governed by the heat transfer rates to and from the n-type and p-type semiconducting pellets.

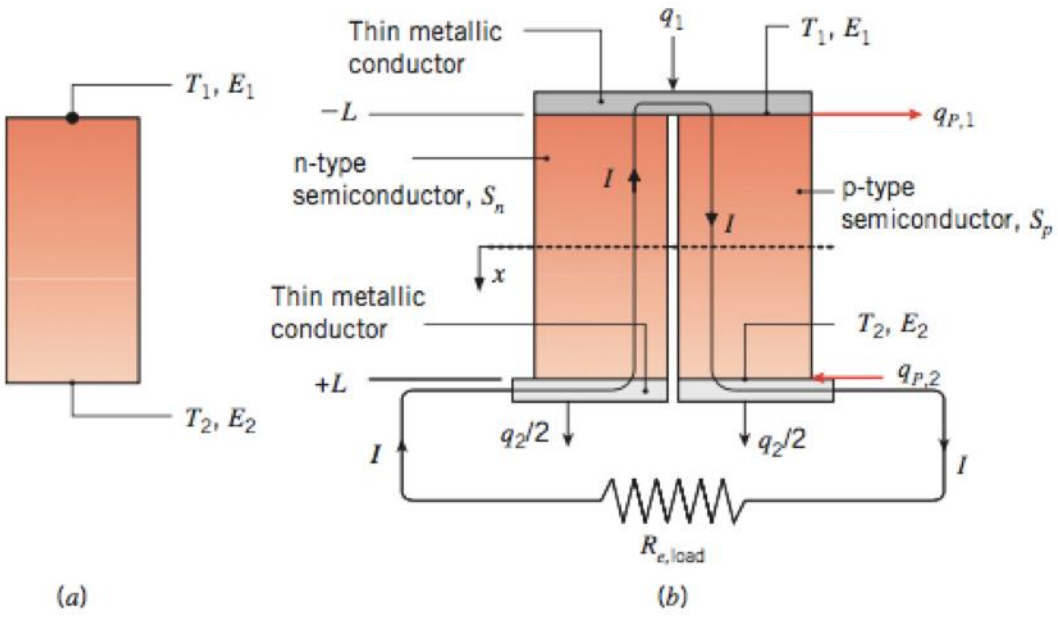

Figure 1-1 Thermoelectric phenomena highlighting the Seebeck effect with a simplified thermoelectric circuit [5].

Electrons are capable of carrying heat and electricity [6]. With a temperature difference between the two faces of a thermoelectric material, such as a TEG, electrons travel from the hot face to the cold face, resulting in heat, and electricity, generation. In practical applications, one side of the TEG is heated via a heat source, and the other side is cooled via a heat sink, resulting in voltage generation. TEGs generate an electrical output from a temperature gradient, with the potential to

result as a renewable energy source driven by the temperature differential in temperature-varying systems, such as HVAC and ICE systems.

TEG technology, as pictured below, incorporates the Seebeck effect with a supply of a heat source and heat sink. The typical TEG has an efficiency of about 5%, which is limited by the Carnot efficiency of a system: $\frac{(T_h - T_c)}{T_h} * 100\%$. While limited by a system's operating conditions, the Carnot efficiency equations provides the correlation between increased temperature differences resulting in greater system efficiency, which is electrical energy generated.

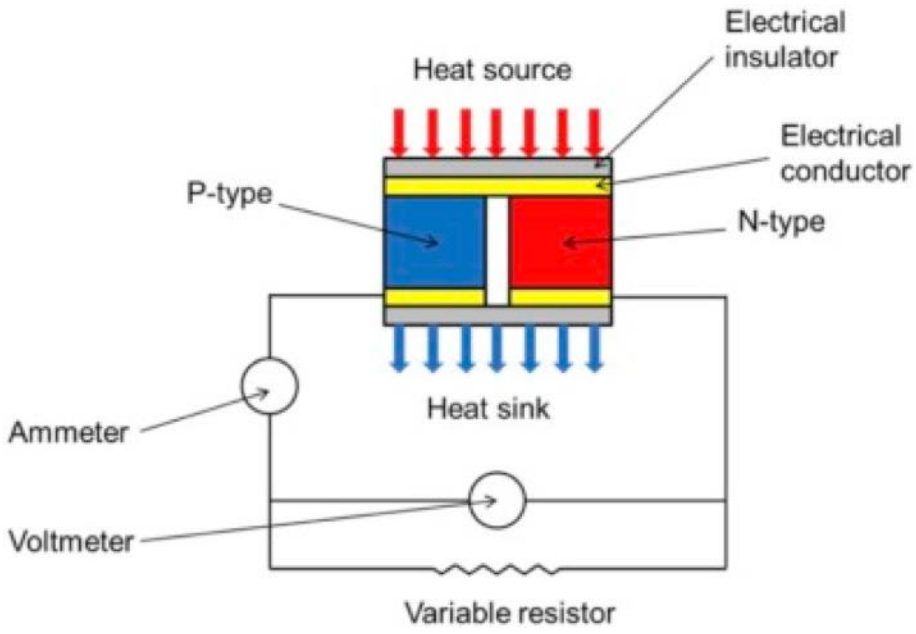

Figure 1-2 Thermoelectric material exhibiting Seebeck Effect given a heat source [3].

Since the 20th century, thermoelectric principles have been explored in real systems to determine the feasibility of increasing energy generation with the Seebeck Effect. Today's reality is one of increasing environmental concerns, as well as a fear of a global energy crisis [6]. As previously noted, approximately 60% of the energy consumed globally is wasted in the form of low-grade

heat. Developing countries use massive bio-fuel furnaces to mitigate global warming, and within laboratory settings, TEGs have been installed to test for improved efficiency. Having seen proven results with TEG incorporation into bio-fuel systems, research is advancing for TEG technology implementation in more waste heat recovery systems. This research is intended to deliver the key objectives related to TEGs in waste heat recovery systems.

With an increased demand to generate energy by renewable means, the TEG technology is examined to indirectly improve efficiency of thermal systems [7]. Thermoelectric materials incite waste heat recovery, which is the recovery and reusing of energy that would otherwise be dissipated into the surroundings of the system. Typical waste-heat recovery systems in which TEGs can be incorporated include steam power plants, exhaust gas, HVAC systems, etc. The benefits of TEG modules incorporated into thermal systems is that they are light and silent, have no moving parts and can convert recycled heat directly into electricity [6]. Beyond these traits, TEGs have the ability to be scaled up to larger systems and are highly durable. The widespread potential for thermoelectric technology is a driving factor behind this research.

A thermoelectric conversion system, shown in Figure 3, normally consists of heat absorbers, TEG modules, and heat sinks, where heat absorbers function as heat collectors to heat up the TEG, and the heat sink functions to dissipate heat from the cold end of the TEG module as rapidly and efficiently as possible to widen the temperature difference between the hot and cold faces, to enhance performance of the TEG module [6]. TEGs are typically paced on the exhaust pipe surface, within an automobile's internal combustion engine, and they are cooled with cold blocks using a coolant, in this case engine coolant. Within the experimental system used in this thesis, the

system is supplied heat, Q_h, at the hot side of the TEG, and cooled via cooling oil on the cold side. The experimental setup of this system features 1.550 kW heat input from a heat fan blower, a designed heat exchanger enclosure with six-plated heat sink fins, an aluminum plate mounted on heat exchanger enclosure, three TEG modules and coolant oil flowing through a water block. The fins are uniformly distributed along the two walls of the HX enclosure [6]. This arrangement guides the flow so that it is impossible for the exhaust gasses to get to the outlet without the development of turbulence [6]. The TEG modules are clamped between the face of the hot-side heat exchangers and the cooling heat sinks with machine screws [6].

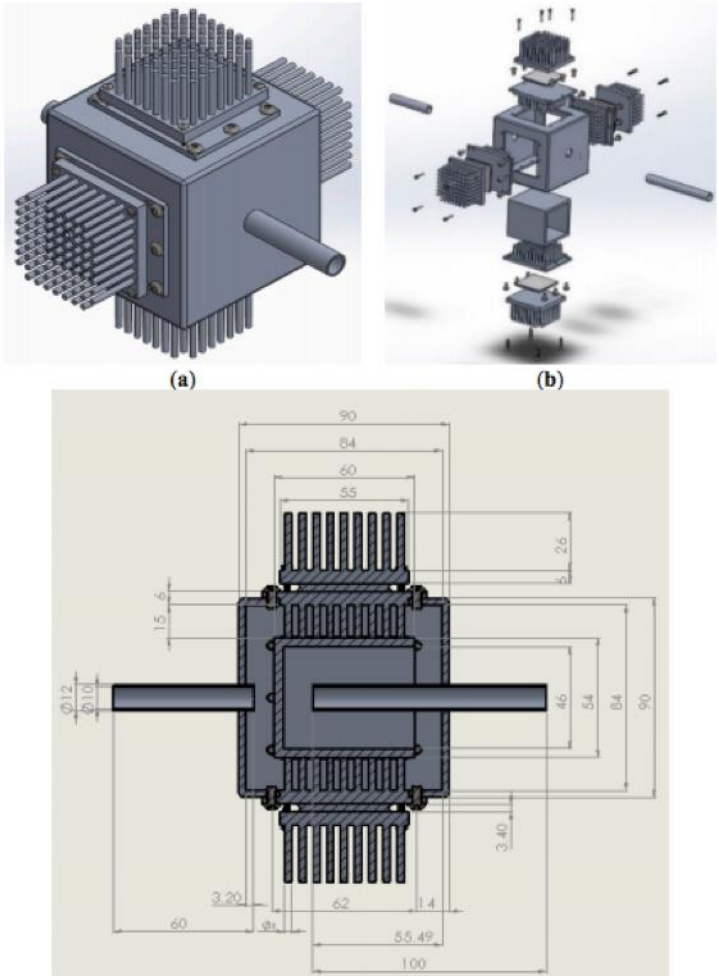

Figure 1-3 Configuration of (a) thermoelectric conversion system, (b) individual parts that mate to form system, and (c) dimensions of the aluminum alloy enclosure [6].

Fin spacing is another major topic explored in design of a HX enclosure. In heat transfer, fins are used to increase the heat transfer from a surface by increasing the effective surface area [9]. Since the use of extended surfaces is often more economical, convenient and trouble free, most proposed application of increasing surface area is adding fins to the inner surface in order to achieve required rate of heat transfer [10]. However, the designer should optimize the spacing or the number of fins on base carefully; otherwise extra fins may disrupt and slow the rate of heat transfer. Although adding numerous fins increase the surface area, they may resist the air flow by reducing the amount of available space for air flow and cause boundary layer interferences which affect the heat transfer adversely [10].

Aluminum alloys are a typical material selection due to their high thermal conductivity as well as lower costs and weight. Fin effectiveness is also enhanced by increasing the ratio of the perimeter to the cross-sectional area [9]. For this reason, the use of thin, but closely spaced fins, is preferred, with the provision that the fin gap not be reduced to a value for which flow between the fins is severely impeded, thereby reducing the convection coefficient [9]. Fin effectiveness is defined by $\varepsilon_f = \frac{q_f}{h*A_{c,b}*\theta_b}$, which provides insight that thin fins, with a smaller area, are better justified for conditions in which the convection coefficient h is small [9]. Experimentally, the convective heat transfer rate through the fin arrays depends on geometric parameters and base-to-environment temperature difference. This research takes into account optimal fin spacing and arrangement within the HX enclosure design.

A difficult aspect of this research, and primary focus of this thesis, is that there are a wide range of operating conditions available within the TEG experimental system. The inputs that can vary include inlet air and coolant flow rates, type of coolant oil and inlet temperatures. Careful analysis of a thermal resistance network is necessary to understand the intermediary resistances and convective heat transfer at the inlet and outlet. Upon establishing the thermal resistance network, a series of inputs can be varied through an established model to determine the outlet temperatures of the air and coolant, the heat transfer from the HX to the oil, and ultimately, the TEG Efficiency.

1.4 Remaining Chapters

Chapter 2 provides a Literature Review of relevant research and progress. The literature review introduces relevant work done on this subject, including progress made on establishing optimal plate fin arrangement, establishing thermoelectric conversion systems, review of waste heat recovery systems in automobile engines and performance tests conducted on TEG systems.

Chapter 3 delivers a detailed overview of the design process for the HX Enclosure. The detailed overview provides each iteration, and detailed design specifications for the final iteration. The chapter reviews how different types of designs and assemblies have been used throughout this research.

Chapter 4 establishes the parameters for the HX System Analysis, including the Performance Test Matrix. These parameters are determined to conduct experimental tests of the system. Chapter 4 also details the experimental procedure.

Chapter 5 performs an analysis of the HX System Experimental results, deriving output parameters of interest in the Performance Matrix.

Chapter 6, Conclusion, summarizes the results of the experimental tests found in this thesis, and discusses future work to be completed on TEG technology.

Chapter 2

Literature Review

This literature review introduces relevant work done on the thesis subject, including progress made on establishing optimal plate fin arrangement, establishing thermoelectric conversion systems, review of waste heat recovery systems in automobile engines and performance tests conducted on TEG systems. The work highlighted in these fields established background knowledge for the work completed in this thesis.

2.1 Fin Arrangement

While designing the HX enclosure, selection of the fin arrangement was a crucial step. Fin arrangement, which can cause temperature to be distributed non-uniformly and decrease heat exchange efficiency, can also affect fluid flow and distribution in different channels of a plate-fin heat exchanger [11]. Previous studies used several methods to analyze fluid flow and heat transfer in heat exchangers with pin fins and corrugated fins, but the effects of fin arrangement on fluid

flow and heat transfer were not heavily analyzed [11]. As the contact position and number of fins vary in different sections, there may be turbulence which can change the flow type and affect fluid turbulence in channels [11]. This is crucial as heat transfer calculations done in this thesis assume fully developed thermal conditions for the air and oil flow. The fin arrangement also affects the temperature distribution, as fins have a certain thickness, and, under the same inlet conditions, channels can be narrower if fins are arranged densely [11]. A denser arrangement results in increased flow rate, allowing a large amount of fluid to flow out of channels without fully transferring heat, reducing heat transfer efficiency in the exchanger [11]. Additionally, fin design is often motivated by a desire to minimize the fin material and/or related manufacturing costs required to achieve a prescribed cooling effectiveness [9]. For the calculations in this thesis, and for simplicity in calculations, it was important to select a proper fin arrangement to ensure uniform temperature distribution.

2.2 TEG Setup

Since TEGs have been discovered as a viable renewable energy source, significant testing has been done to establish the practicality of the technicality. Many current studies have addressed waste heat recovery from engines using TEG devices and many have claimed patents [6]. Studies on thermoelectric generation by the recovery of engine waste heat emphasize integrated thermos-electric conversion devices and performance simulations [6]. In the study by Chienkuo Technology University in Taiwan, the thermoelectric conversion system consists of heat absorbers, TEG modules, and heat sinks. The heat absorber heated up the TEG, while the heat sink dissipated heat from the cold end of the TEG module. The exhaust gases were brought through a circuitous path,

which is forced past the pin-fin heat absorbers. The resulting turbulence enhanced heat exchange between the hot exhaust gases and the extensive surface of the heat exchangers [6]. The fin pins were all the same length and made contact with the baffle box in the center of the chamber, forcing the flow to the outlet while developing turbulence. In that study, the experimental setup for generation performance test of a single TEG module is shown below.

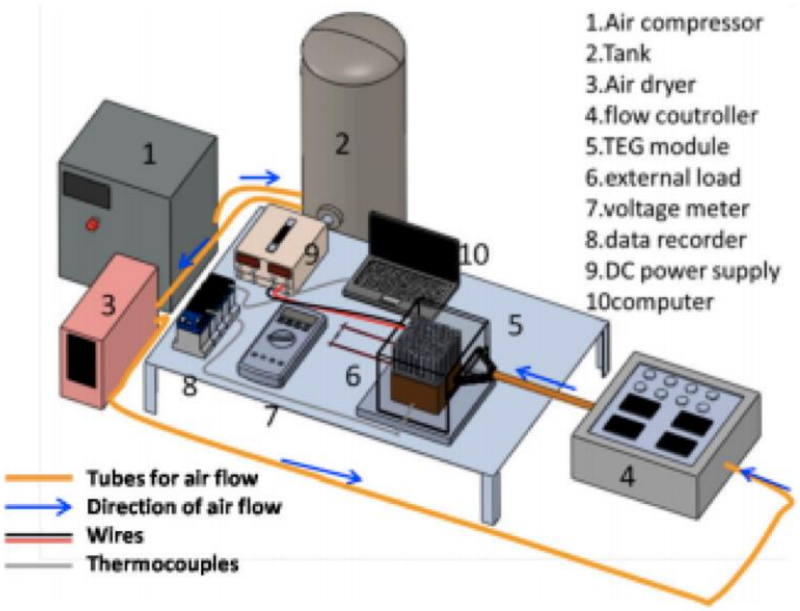

Figure 2-1 Experimental setup used for the single chip TEG experiment [6].

The Chienkuo setup includes an air supply, a TEG module, a test section with heating and cooling devices, and data acquisition tools. The experiment investigated power generation of a TEG module, represented by an output wattage. The experimental results indicate that when the temperature difference between hot and cold faces of the TEG, $\Delta T = T_h - T_c$, is greater, there is a greater TEG power output. Power in the system is $P = V^2/R$, where R is a load resistor (Ω) and V is the output voltage (V), so a larger load resistor corresponds to a greater TEG output voltage. The correlation between maximum power generation and temperature differences was defined

as: $P = 0.0002 * (T_h - T_c)^2$. This correlation supports prior theoretical research signaling that an increased temperature gradient results in greater TEG power generation.

2.3 Real World Applications

In automobile engine systems, several groups have introduced thermoelectric conversion systems. The opportunity for efficiency improvement is illustrated the diagram below, highlighting the energy flow diagram within a vehicle. As highlighted, the 40% lost efficiency from exhaust gas can be decreased by the implementation of thermoelectric technology. Large multinational car companies such as BMW, Ford, Honda, etc., have demonstrated interest in exhaust heat recovery, developing systems that make use of TEGs. The typical design locates the TEG placed on the exhaust pipe surface, the hot side, and are cooled with cold blocks using engine coolant, the cold side. The Ford system heat exchanger uses many small parallel channels lined with thermoelectric material for the exhaust gases to pass. Liquid cooling is used in this case [5].

This system is rated to produce a maximum of approximately 400 W with 4.6 kg of thermoelectric material [5]. The Renault system is to be used on a diesel truck engine. It has dimensions of 10 cm × 50 cm × 31 cm [5]. This system uses a counter flow heat exchanger arrangement using liquid cooling. A combination of high temperature TEGs at the high temperature end and low temperature TEGs at the low temperature end were used [5]. The studies found an appropriate way to improve the overall efficiency of fuel used in a car to recover wasted exhaust gas with the implementation of TEGs. The expected impact from efficiency calculation is ~1 mpg (5%) fuel economy improvement for a typical Suburban vehicle. Reviewing this study asserted the practical

applicability of TEGs, and the results of this thesis took into account the system setup and fin arrangement to develop the experiment.

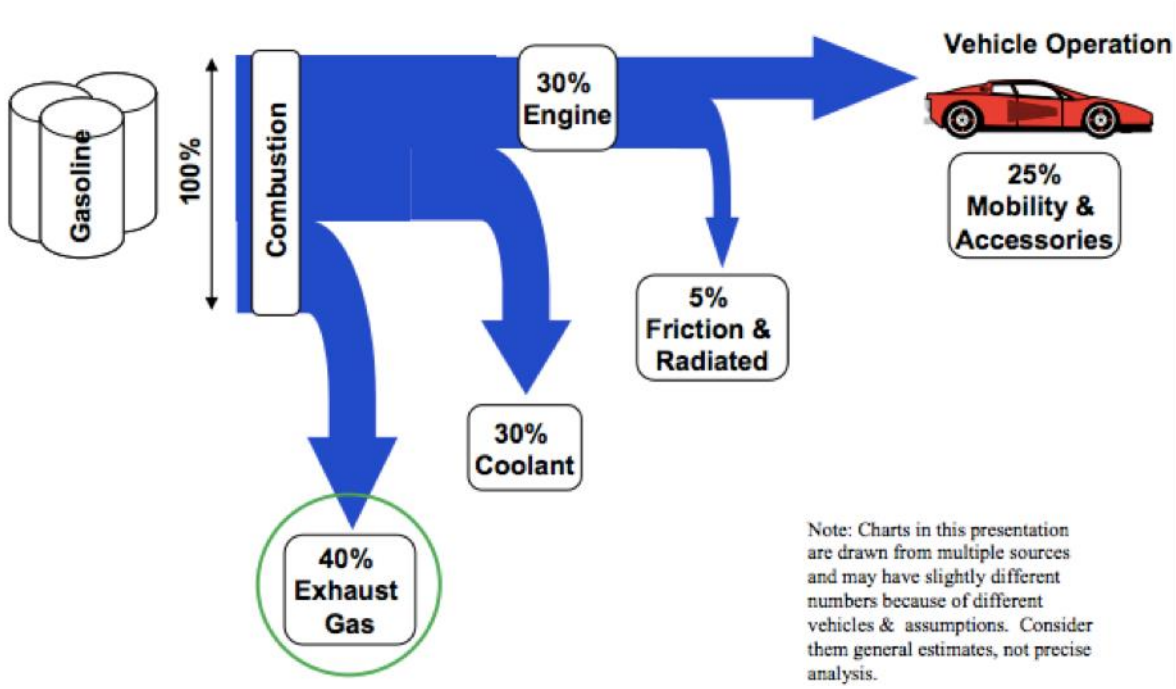

Figure 2-2 Automotive energy flow diagram, highlighting 40% efficiency lost through exhaust gas [12].

Chapter 3

HX Enclosure Design

Prior to the experimental setup, it was necessary to design an enclosure to enhance heat transfer and reach the TEGs. A focus of this thesis was to create an HX Enclosure, which would include heat sinks to enhance heat transfer through the system and towards the TEG modules. This chapter provides a detailed overview of this enclosure, and of each iteration in the design process.

3.1 HX System Overview

The setup of the initial model for the enclosure system, a heat fan blower funneling air at 793K into a cylindrical pipe, did not practically allow the air to flow through a system and to the TEGs for power generation. For the experimental system, the primary task was to design an HX enclosure, which would serve as the starting point for heat delivery to the TEG and for development of the thermal resistance network. The secondary task was to minimize heat loss to the surroundings when the system was running. Prior to developing a precise design, the system was defined and is shown via a sketch below. The sketch provided clarity of the system and its components, for one heat sink, allowing the author to quantify the various modes of heat transfer taking place.

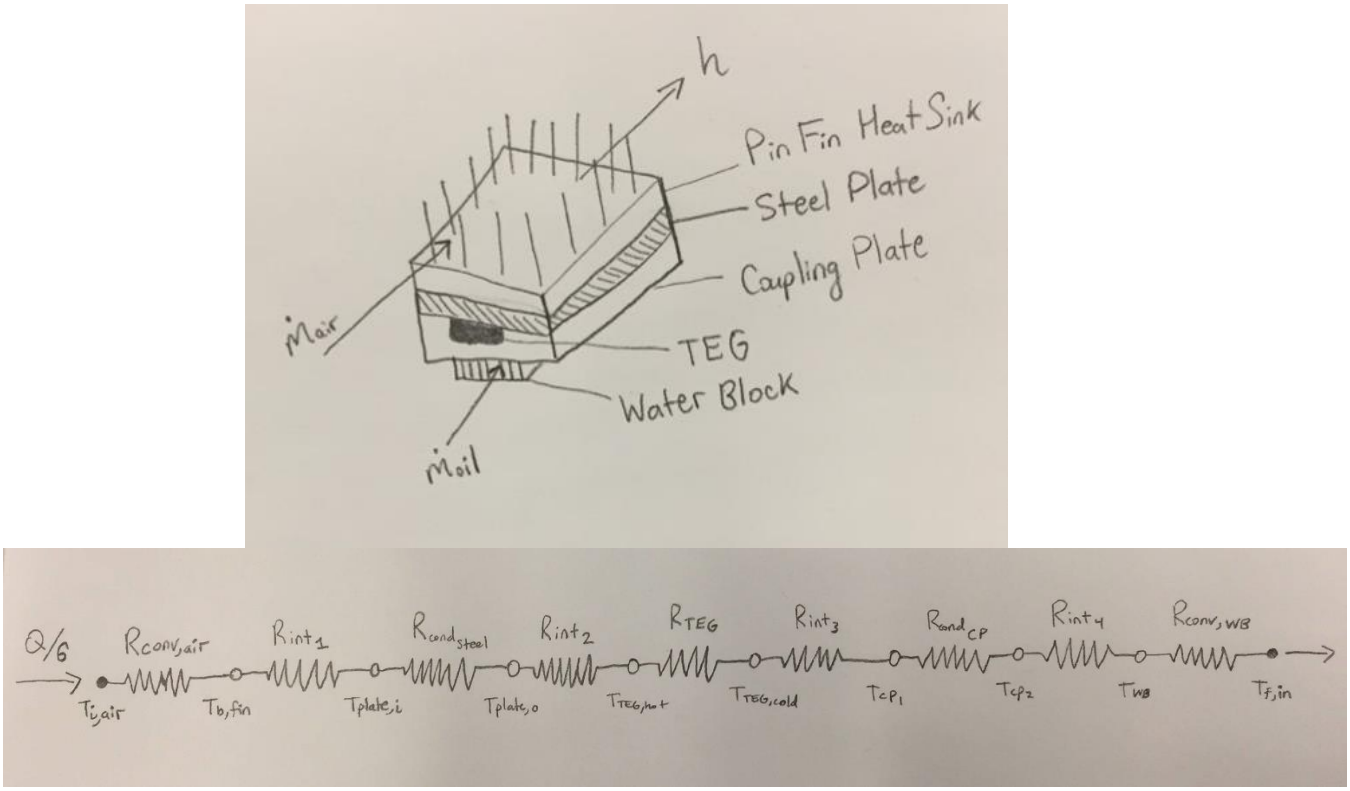

Figure 3-1 Thermal Resistance Network Corresponding to heat sink setup

After understanding the Heat Sink setup, the author devised a thermal resistance network. The heat input in this system is Q/6, due to the assumption of even heat distribution between the six heat sinks in the final design. The modes of heat transfer in the thermal resistance network are convection and conduction, where $h = Convection\ coefficient\ [\frac{W}{m^2 * K}]$. The network experiences resistance due to convection, conduction, and "interface resistance," at the contact points of the Finned Heat Sink and Steel Plate, the Steel plate and the TEG, the TEG and the Coupling Plate, and the Coupling Plate and the Water Block. Each resistance is calculated in "Appendix A: Thermal Resistance Network Calculations." The calculations showed that a significant percentage of the total resistance, 94.4%, was due to convection, highlighting that conduction and interface resistances were near-negligible. However, the author included the

effects of these resistances in the experiments, for accuracy of the overall resistance (UA), corresponding input heat (Q), and subsequent outputs described in Chapter 4.1.

Furthermore, knowing the number and the arrangement of the heat sinks, the author configured an overall thermal resistance network. As shown in Figure 3-2, the six heat sinks act as parallel resistances in the overall thermal resistance network, in which R_1 through R_6 are equal to the total resistance through each Heat Sink Setup. This network setup allowed the author to conduct a theoretical calculation of the UA value, due to the various modes of heat transfer. These calculations are expanded upon in Appendix A.

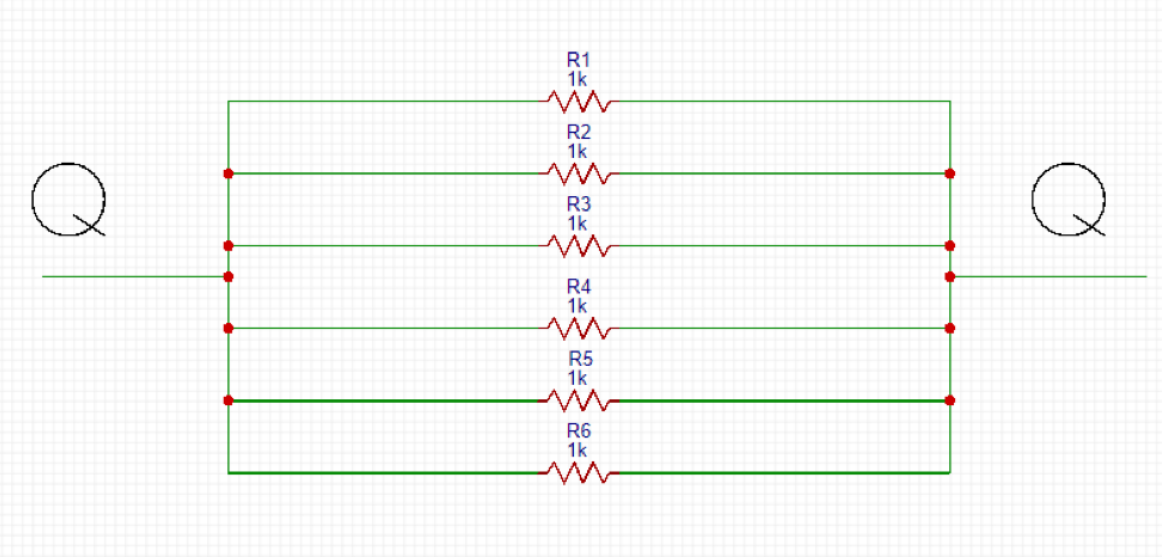

Figure 3-2 Overall Thermal Resistance Network

The system featured a heat fan blower delivering 1.550 kW of energy through a 2.43-in pipe, but required an enclosure to 1) enhance heat flow and heat transfer to the subsequent system components, and 2) minimize dissipated heat loss to the surroundings. The HX enclosure was limited by the geometric constraints of the fins to be placed in the enclosure and the pipe diameter. These constraints included plate fins 40mm in height, 80mm by 80mm in base area, a required

minimal spacing of 0.025” (0.635mm) between each plate fin to ensure manufacturability and proper assembly of parts, and 2.43” (61.7mm) pipe diameter. From thermodynamics, the volumetric flow rate is defined by $\dot{V} = \frac{dV}{dt}$. This equation shows that a sudden change in volume, which would mean *dt* is small, results in disruption of the volumetric flow rate. The calculations and experiment required steady flow, meaning geometric dimensions of the enclosure cannot experience sudden changes in volume. After establishing these geometric and practical design constraints, the author moved forward with the design of the enclosure. The geometry of the enclosure was designed to maximize the interior space within those restrictions.

3.2 Initial Prototypes

The HX enclosure consists of: bended sheet metal, six heat sinks, two octagonal plates, and four bolts. When designing the HX enclosure to enable and enhance heat delivery through mounted plate fins, there were several SolidWorks tactics applied to simplify the design process. The use of a geometrically precise design, with exact placeholders for the mounted plate fin heat sinks, standard manufacturer hole sizes and minimizing material usage for cost-effectiveness were key components of the design.

The heat sink, shown below, was designed to replicate the heat sink purchased from the selected vendor. The purpose of the heat sink is to enhance air flow through the HX enclosure so that maximum heat input, Q, can be carried out throughout the system and into the TEG. The heat sinks are placed within the hexagonal enclosure, with three heat sinks per side, to maximize the heat Q carried to the TEG modules. The heat sink was designed using linear patterns to create geometric

exactness, which would carry over to the stage of mating the heat sinks to the HX enclosure. An important note made in the later stages of this thesis is that the heat sink had a staggered alignment of fins, which would impact overall fin efficiency. In the experiments and pre-test analyses, the author assumed an aligned fin arrangement, allowing for simple calculation of fin efficiency.

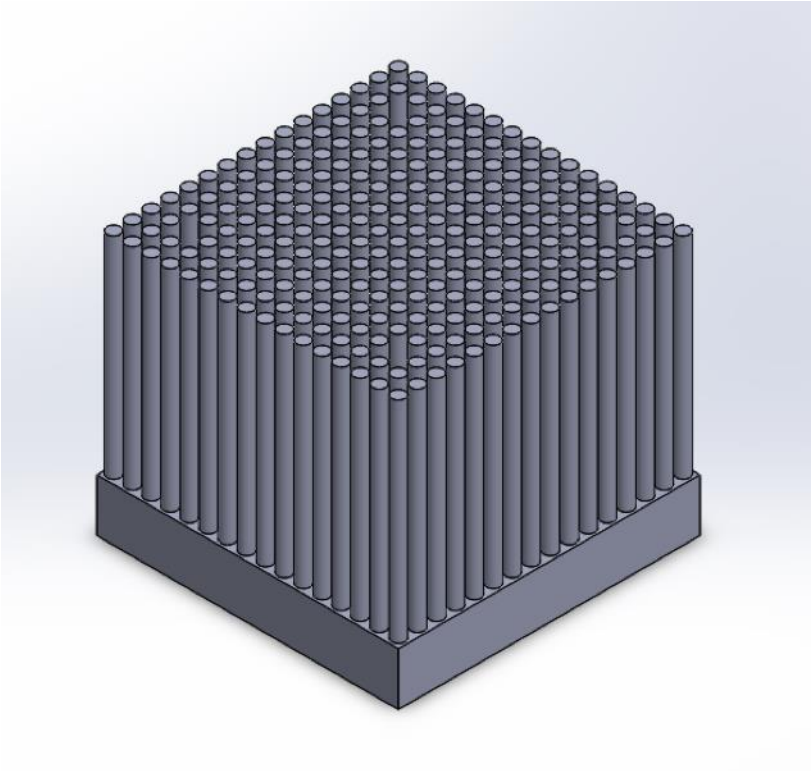

Figure 3-3 SolidWorks model of a pin-fin heat sink.

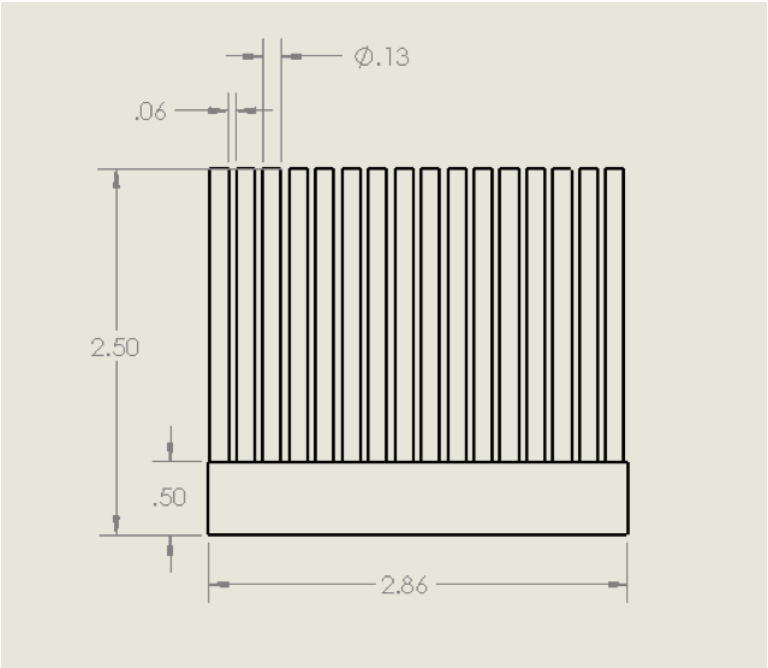

Figure 3-4 Corresponding dimensions of the pin-fin heat sink

Recall that fins are used to increase the heat transfer from a surface by increasing the effective surface area [9]. However, to quantify exactly how the usage of fins, and specifically the pin fins used in the experimental setup, the author incorporated fin effectiveness into convection calculations. Due to the simplicity of the fin arrangement, fin efficiency was calculated using the "Fundamentals of Heat and Mass Transfer" formula: $\eta = \tanh(mL_c) \Big/ (mL_c)$ [9]. In this thesis's situation with pin fins, the term mL_c can be defined as $\left(\frac{2h}{kA_p}\right)^{1/2} * L_c^{3/2}$, where L_c can be defined as the corrected fin length, h is the convection coefficient, k is the metal's thermal conductivity and Ap is defined as the corrected fin profile area. For pin fins, $A_p = \pi D L_c$ and $L_c = L + (\frac{D}{4})$ [9]. Fin efficiency's importance in the remaining calculations is that it allowed the author to make an assumption on the theoretical heat (Q) that would be transferred from the heat fan blower's air through the remaining stages of the experimental design.

With a pin-finned heat sink selected, the next step in this thesis was to conduct material selection. The engineering principle the author focused on was Thermal Conductivity. Thermal conductivity, denoted as *k*, is defined as the property of a material to conduct heat [9]. Thermal conductivity is evaluated in terms of Fourier's Law for heat conduction: $\mathrm{Q} = -\mathrm{k} * \mathrm{A} * (\frac{\mathrm{dT}}{\mathrm{dx}})$. The constant k is the thermal conductivity constant, which is larger for materials that transfer heat well, and small for materials that transfer heat poorly. In this project, the greater the thermal conductivity of the metal, the more proficient it is at removing heat away through the system. [13]. Metals are materials that have the highest conductivity at an affordable cost [13].

Shahzaib investigated several options for metals such as copper, aluminum, steel, etc. From the metals, aluminum was one of the most common metals used to make heat sinks. Aluminum is also fairly cheap and lightweight. Having lightweight material is crucial as weight induces stress. For this system, having lightweight aluminum heat sinks would reduce the risks of stress induced on the enclosure. Aluminum also possessed a high thermal conductivity of 237 watts per meter Kelvin (W/m*K), and a melting point capable of withstanding the maximum temperatures in this system [9]. Comparatively, the metal copper has a thermal conductivity of 401 W/m*K, which makes the copper more conductive than aluminum. However, copper is about three times as dense as aluminum, with a density of 8933 kg/m3 versus aluminum's density of 2702 kg/m3. The increased thermal conductivity of copper did not hold greater importance than the increased weight of copper, so the pin-finned heat sinks were selected to be manufactured with aluminum.

The HX enclosure went through several iterations, which began with the figure below. The figure below highlights the geometric dimensions of the enclosure, as well as the proposed shape of the

enclosure. The enclosure has a rectangular extrusion in which the six heat sinks would be placed, as highlighted in the cross-sectional view. This design was made stressing the placement of the heat sinks, and geometric constraints. Several issues with the model included its manufacturability, as there was no way to mount the enclosure to the experimental system nor was there geometric symmetry in many parts of the assembly, leaving the prototype prone to human welding errors. This manufacturing issue along with several not having designed SolidWorks parts with standard sizing, led to drafting a second prototype.

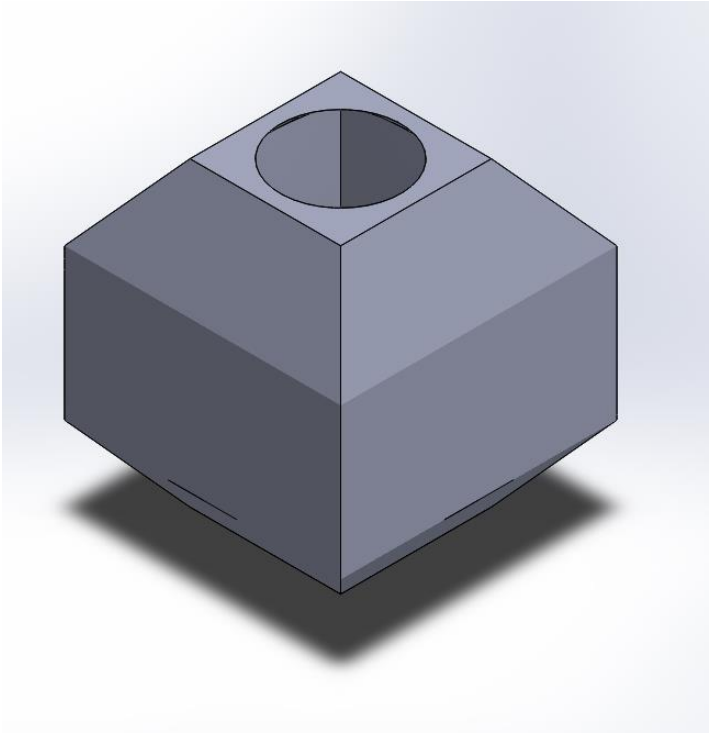

Figure 3-5 Initial Prototype of HX Enclosure.

Upon the first iteration, several modifications were put in place. The modifications that were made to the first prototype SolidWorks included a re-dimensioning of the enclosure. The enclosure outline transitioned from a rectangular enclosure to a symmetrical, hexagonal enclosure. The heat transfer principles involving uniform heat distribution to the heat sinks, enhancing heat flow with

the optimal arrangement of heat sinks as discussed in the Literature Review, and gradual change in volume were satisfied in this iteration of the enclosure design. A “lip” surrounding enclosure was implemented to bolt the two halves of the HX enclosure together, making heat loss to the surroundings negligible.

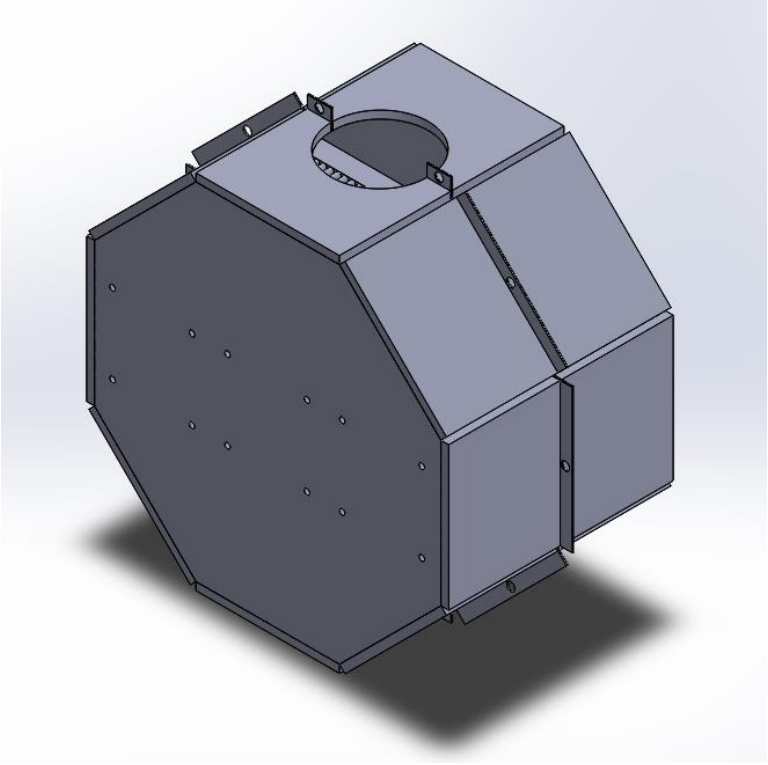

Figure 3-6 Second iteration of the HX Enclosure - full view.

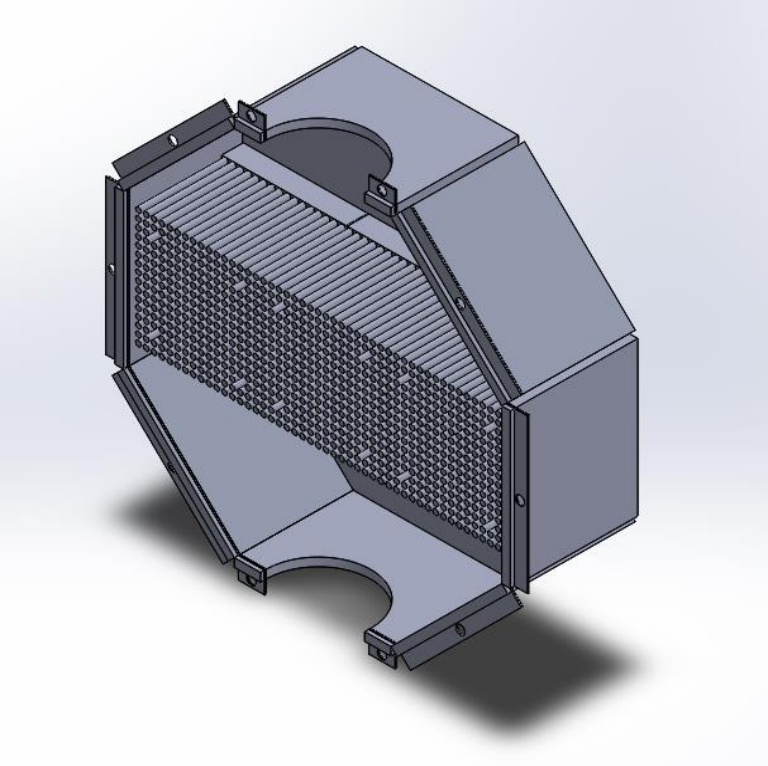

Figure 3-7 Second iteration of the HX Enclosure - cross-sectional view

3.3 Final Design

A final iteration of the HX Enclosure highlights a key difference in the mounting method: running bolts through the enclosure. The “lip” enclosure did not ensure the stability desired for the system. To correct this issue, the author designed four bolts to run through the enclosure, essentially allowing the enclosure to maintain stability as system tests were conducted. The design effort required a practical application of bolts to ensure the HX enclosure stays in place and steady throughout the experimental phase. This effort was a crucial step as moving to designing the thermal resistance network and preparing a performance test matrix depended on successful design and installation of the HX enclosure.

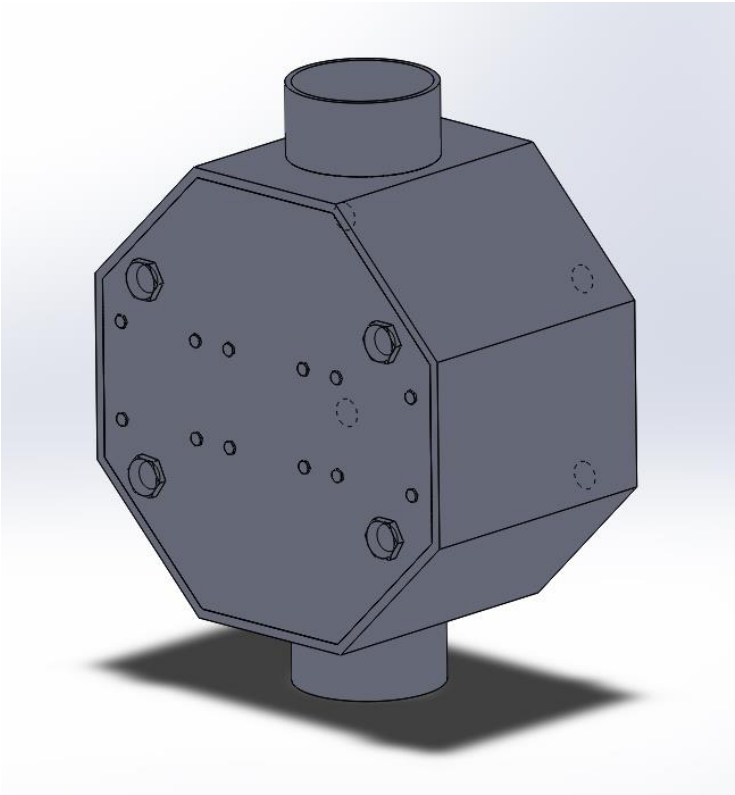

Figure 3-8 Final SolidWorks model of the HX Enclosure.

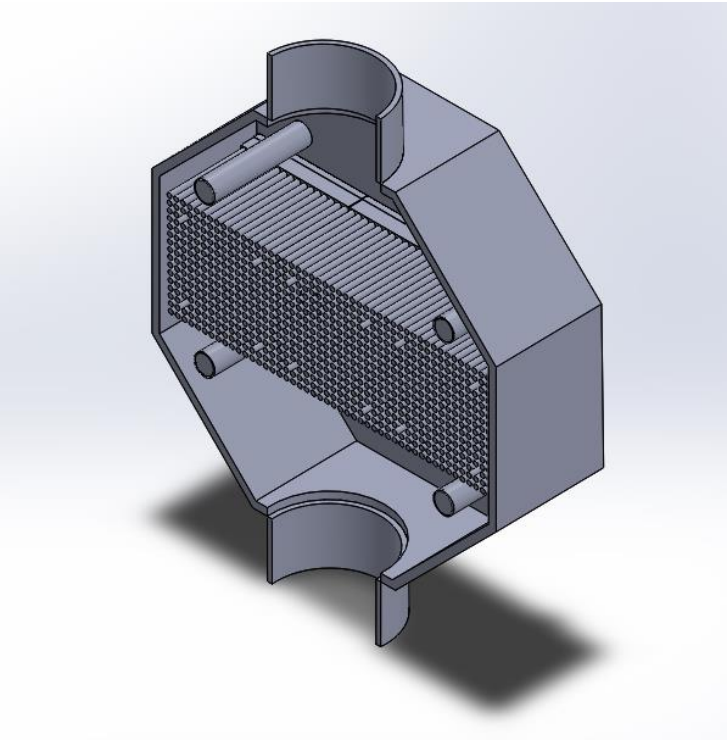

Figure 3-9 Final SolidWorks cross-sectional model of the HX Enclosure.

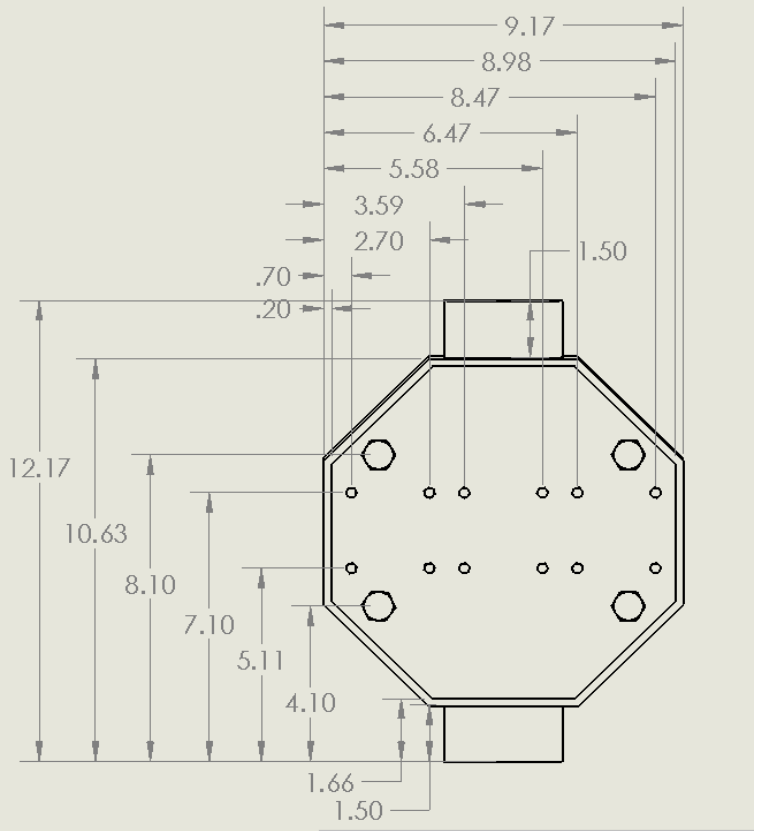

Figure 3-10 Dimensions of final design of the HX Enclosure.

Due to the nature of the enclosure design, Dr. Rattner and Shahzaib explored several welders as the preferred form of manufacturing. Additive manufacturing was not explored as the complexity of the design as well as the practical usage of the enclosure made the additive manufacturing process unfeasible. The inlet air temperature from the heat fan blower is 793K, which would melt the additive manufacturing material. After completing the SolidWorks design, both as an assembly and deconstructing to individual parts, Shahzaib found a suitable vendor for constructing and welding the individual parts of this enclosure. To properly weld the enclosure, aluminum slab was welded into the bended sheet metal, with a circular 2.43” opening to be connected to the cylindrical pipe of the system. Then within both sides of the enclosure, a “placeholder” was created for each

of the heat sinks to be situated and screwed into the enclosure walls. Beyond this, there were 4 larger 0.75” holes on each of the enclosure walls so that the HX enclosure can be bolted in place of the experimental system.

There were several strengths to the final iteration of the HX enclosure. These strengths included ability to be welded by a standard vendor, avoiding increased costs of a specialized weld shop. The symmetry of the design ensured uniform heat distribution, which satisfied assumptions made for theoretical thermal resistance network calculations. The individual parts and standard sizing of holes allowed mating and welding to occur seamlessly, and bolt the designed enclosure onto the cylindrical pipe with ease. Lastly, the individual parts were designed to match the specified geometric design constraints, increasing ease of assembly. The individual parts are provided in summary with the Bill of Materials below.

ITEM NO.	PART NUMBER	DESCRIPTION	QTY.
1	Sheet Metal - Side Bended	Sheet Metal sides manufactured with aluminum, thickness = 0.20". Manufactured via bending sheet metal at the specified locations.	1
2	Sheet Metal - Octagon Plate	Standard Hole sizing and note the sockets to place the heat sinks.	2
3	Thesis_Heat_Sink	Heat sink procured from vendor, designed for assembly purposes.	6
4	Pipe Extrusion	0.25" thickness, designed to mount HX Enclosure onto heat blower system	2
5	Bolt	Bolts of standard size designed for assembly purposes (will be purchased from vendor)	4
6	Hollow Cylinder	Casing for Bolts, designed for assembly purposes.	4
7	Screw	Standard-sized screws will be purchased from vendor, designed for assembly purposes.	24

Figure 3-11 Bill of Material for HX Enclosure

Chapter 4

HX System Setup

Upon manufacturing the final iteration of the HX enclosure, the author developed a performance test matrix. This matrix setup input parameters to evaluate in the system tests. Prior to running tests, a theoretical model based on the thermal resistance network was calculated. This chapter also details the experimental process, and the test results.

4.1 Characterization/Performance Matrix

The performance matrix set up of test conditions allowed the author to test an array of varying inputs for a corresponding output. In this experiment, the varying inputs included inlet temperatures of air and oil and the inlet flow rates of the air and oil. The constant inputs included the heat sink and water block geometry, and the type of coolant oil. Ultimately, the goal of the experiments was to determine the efficiency of the TEG and the power output. To derive these parameters, the author recorded the resulting outlet temperatures and overall system resistance. From this point, the heat transfer equation $\mathrm{Q} = \mathrm{UA} * \mathrm{LMTD}$ was utilized to determine the power output and consequentially, the TEG's efficiency. In the previous equation, UA is derived from the thermal resistance network model, and the LMTD is log mean temperature difference. The LMTD approach is defined by several assumptions, which include:

1) The heat exchanger setup has only two streams [14].

2) Heat exchange with the surroundings of the system is negligible [14].
3) The overall heat transfer coefficient between the streams is constant throughout the heat exchanger [14].

The LMTD value is determined by LMTD = $(\Delta T_1 - \Delta T_2) / \ln (\Delta T_1/\Delta T_2)$, in which the various temperature differences are determined by the experimental inlet temperatures. ΔT_1 is defined as $T_{air,in} - T_{oil,out}$, while ΔT_2 is defined as $T_{air,out} - T_{oil,out}$. It is important to note that generally, T defines ΔT. With the input and output test parameters defined, the author developed the test matrix as shown below.

INPUT VARIABLES		OUPUTS								
Variable Changed	New Value	T_air,out	T_oil,out	LMTD	UA	Power (Q)	HT to Oil	Heat loss from HX	TEG Efficiency	Uncertainties
T_air (K)	400									
	500									
	600									
	700									
	900									
T_oil (K)	150									
	200									
	250									
	300									
	350									
	400									
mdot_air (kg/s)	0.0500									
	0.0600									
	0.0800									
	0.0900									
	0.1000									
mdot_oil (kg/s)	0.0750									
	0.0100									
	0.0150									
	0.0225									
	0.0250									

Figure 4-1 Performance Matrix with sample inputs varied, along with the outputs of interest.

From the above diagram, the primary input variables were varied one at a time (with all other inputs remaining constant). The inputs varied included the inlet air temperature, the inlet oil temperature, the inlet mass flow rate of air and the inlet mass flow rate of oil. It was interesting to

note that there was an inverse relationship between inlet air temperature and mass flow rate. This inverse relationship arose from the fact that as inlet temperature increases, the fluid's density decreases. Tying this to the fact that mass flow rate (in *kg/s*) is derived from the density multiplied by the volumetric flow rate ($\dot{m} = \rho * \dot{V}$), the author determined the validity of this relationship. For each of the inputs, the values are varied both below and above the default input values to isolate the potential impact of each input variation. The outputs defined were the parameters of interest and were recorded for each of the varied inputs.

Furthermore, this setup allowed for step-by-step calculations of the power output (W) and the TEG efficiency. Beyond these key measurements, the author also derived the heat transfer to the oil, as well as the subsequent heat loss in the HX. After the test matrix setup, Shahzaib and Yue Cao physically mounted the HX enclosure, water block, Pitot tube and thermocouples for instrument readings onto the cylindrical heat blower system to conduct experiments and analysis.

4.2 Experimental Setup and Initial Model

The entire system consisted of a TEG/Oil Loop. The incoming oil was looped to the HX system and through a desorber. The heat came into the HX enclosure via a steady fan blower, with adjustable mass flow and temperatures for the hot air. From this point, heat went towards power generation for the TEGs and heat transferred to the oil loop.

Prior to conducting the experiment, a set of calculations were conducted based on the initial inputs. These calculations served as a baseline for conducting experiments while varying inputs according

to the Performance Matrix in 4.1, and more importantly, determining how variation of each input affects the output metrics.

Calculation Development [Appendix B]:

Appendix B provides a complete overview of the simultaneous equations used to derive the log-mean temperature difference (LMTD), overall resistance (UA), outlet air and oil temperatures, and Q_{air} and Q_{oil}. Due to the nature of simultaneous equations, the Engineering Equation Solver (EES) program was used to solve for these outputs. The full code is included in Appendix B.

Variable Definition:

$\dot{m}_{air} = Mass\ flow\ rate\ of\ inlet\ air\ [\frac{kg}{s}]$

$\dot{m}_{oil} = Mass\ flow\ rate\ of\ inlet\ oil\ in\ water\ block\ [\frac{kg}{s}]$

$T_{air,in} = Temperature\ of\ inlet\ air\ [K]$

$T_{oil,in} = Temperature\ of\ inlet\ oil\ in\ water\ block [K]$

$T_{air,out} = Temperature\ of\ outlet\ air\ [K]$

$T_{oil,out} = Temperature\ of\ outlet\ oil\ in\ water\ block [K]$

$h_{1,air} = Specific\ enthalpy\ of\ air\ at\ T_{air,in}\ \left[\frac{kJ}{kg}\right]$

$h_{1,oil} = Specific\ enthalpy\ of\ air\ at\ T_{oil,in}\ \left[\frac{kJ}{kg}\right]$

$h_{2,air} = Specific\ enthalpy\ of\ air\ at\ T_{air,out}\ \left[\frac{kJ}{kg}\right]$

$h_{2,oil} = Specific\ enthalpy\ of\ air\ at\ T_{oil,out}\ \left[\frac{kJ}{kg}\right]$

$c_{p,air} = Specific\ heat\ of\ air\ at\ T_{air,in}\ \left[\frac{kJ}{kg * K}\right]$

$c_{p,oil} = Specific\ heat\ of\ oil\ at\ T_{oil,in}\ \left[\frac{kJ}{kg * K}\right]$

$LMTD\ = Log\ mean\ temperature\ difference$

$UA = Overall\ system\ resistance\ [\frac{W}{K}]$

$Q_{air} = Heat\ transfer\ rate\ from\ air\ to\ the\ HX\ [kW]$

$Q_{oil} = Heat\ transfer\ rate\ to\ the\ oil\ [kW]$

Assumptions:

$\dot{m}_{air} = 0.0730\ [\frac{kg}{s}]$

$\dot{m}_{oil} = 0.02618\ [\frac{kg}{s}]$

$T_{air,in} = 794\ [K]$

$T_{oil,in} = 393\ [K]$

$h_{1,air} = 811.0\ [\frac{kJ}{kg}]$

$h_{1,oil} = 261.1\ [\frac{kJ}{kg}]$

$c_{p,air} = 1.098\ [\frac{kJ}{kg * K}]$

$c_{p,oil} = 2.30\ [\frac{kJ}{kg * K}]$

Calculations were carried out based on the stated assumptions to determine several key output variables: namely, power output, Q. The initial value of Q was later used to analyze key metrics such as heat loss from the HX enclosure, heat transfer to the oil and TEG efficiency from the system energy balance. For the UA value, the same resistance network calculations were utilized from Appendix A. Using this value, as well as EES to solve a set of 7 simultaneous equations, the key outputs were determined (with the complete calculations listed in Appendix B).

$$h_{2,air} = \frac{Q}{\dot{m}_{air} * c_{p,air}} + h_{1,air}$$

$$h_{2,oil} = \frac{Q}{\dot{m}_{oil} * c_{p,oil}} + h_{1,oil}$$

$$T_{air,out} = \frac{h_{2,air} - h_{1,air}}{c_{p,air}} + T_{air,in}$$

$$T_{oil,out} = \frac{h_{2,oil} - h_{1,oil}}{c_{p,oil}} + T_{oil,in}$$

$$UA = \left(\frac{1}{6 * R_{TOT}}\right)$$

$$LMTD = \frac{\left(T_{air,in} - T_{oil,out}\right) - \left(T_{air,out} - T_{oil,out}\right)}{\ln\left(\frac{T_{air,in} - T_{oil,out}}{T_{air,out} - T_{oil,out}}\right)}$$

$$Q_{air} = UA * LMTD$$

$$Q_{oil} = \dot{m}_{oil} * c_{p,oil} * \Delta T_{oil}$$

$$Q_{air} = 1.550\ kW$$

$$Q_{oil} = 0.756\ kW$$

Calculating the value of Q_{air} allowed the author to understand the maximum power output for the TEG, as well as gage the potential heat loss occurring during the system tests. The TEG is only able to convert a small fraction of the heat flow between the TEG/Oil Loop. The model's results were later compared with the experimental results to understand where heat was being transferred to within this system and the discrepancies between the theoretical and experimental TEG power outputs.

4.3 Experimental Procedure and Results

After calculating theoretical values based on a set of initial inputs, the author moved to setting up the system and running experimental tests. With help from Shahzaib and Yue, two PhD students on the team, the assembled system displayed no functional failures, leaks, etc. This complex assembly was crucial to the ability to conduct and analyze experimental tests. The experimental procedure was detailed to ensure a standardized procedure, minimizing forms of human error.

The waste heat recovery system included the TEG/HX Enclosure and the Oil Loop, and tests were conducted at various fan blower settings, by altering the temperature and mass flow rate of the air blower. The process for the experimental tests is as followed:

Table 4-1 Experimental procedure for starting and stopping waste absorption facility

1.	Turn on the main system's power and Blower power. Connect the USB Cable to the desktop.
2.	Open the LabVIEW monitoring program "Absorption."
3.	Turn the Emergency Stop knob to the right (clockwise).
4.	Turn on the Load Device. Flip the "INSTS" and "Pump" switch on (Up).
5.	Run the LabVIEW monitoring program.
6.	Turn on the fans for the oil loop.

7.	Attach the curtains and turn on ventilation system.
8.	Turn on the heater, and observe data till it stabilizes. Record these steady state conditions. Continue to run tests for desired input blower settings.
9.	After having completed the tests, follow these steps to safely turn off the system.
10.	Turn off the Heater. After several minutes, turn off the fans for the oil loop.
11.	Turn off the load device.
12.	After the oil loop has cooled, turn off the "INSTS" and "Pump" switch (Down).
13.	Stop running the LabVIEW monitoring program.
14.	Push the Emergency Stop Button.
15.	Disconnect the USB Cable and turn off the blower power and main system's power.

Following this procedure ensured the results would represent true steady state system values, allowing for a proper system analysis. The author collaborated with Dr. Rattner to conduct several tests for the system, varying the mass flow rate and temperature of the blower's air. The relevant experimental readings are included below, highlighting the test runs without insulation. These tests were analyzed in energy balances to determine the heat transferred to the oil, heat delivered to the TEG and the value of the heat lost to surroundings. The experimental values taken from the LabVIEW monitoring program allowed the author to not only calculate the output parameters of interest, but also compare experimental results with the values from the author's initial model.

Table 4-2 Outputs under maximum temperature and mass flow rate of heat blower

Item	Value	Unit
Air inlet temp	286.6	C
Air exhaust temp	175.8	C
Exhaust velocity	899.8	FPM
Oil inlet temp	52.6	C
Oil outlet temp	68.9	C
Oil pressure	161.1	kPa
Oil mass flow rate	1.44	LPM
TEG inlet temp	51.9	C
TEG outlet temp	69.1	C
HX Pressure diff	34.3	Pa
Load voltage	23.8888	V
Load current	0.147	A
Load power	3.505	W

Load resistance	162.576	Ω
Desorber OO Temp	54.1	C
Desorber OI Temp	68.9	C

Table 4-3 Outputs under maximum temperature and 50% mass flow rate of heat blower

Item	Value	Unit
Air inlet temp	381.9	C
Air exhaust temp	192.7	C
Exhaust velocity	635.2	FPM
Oil inlet temp	58.2	C
Oil outlet temp	76.8	C
Oil pressure	154.6	kPa
Oil mass flow rate	1.49	LPM
TEG inlet temp	57.5	C
TEG outlet temp	77.3	C
HX Pressure diff	17.0	Pa
Load voltage	23.8888	V
Load current	0.171	A
Load power	4.081	W
Load resistance	139.647	Ω
Desorber OO Temp	59.7	C
Desorber OI Temp	76.2	C

Table 4-4 Outputs under 50% maximum temperature and 50% mass flow rate of heat blower

Item	Value	Unit
Air inlet temp	209.9	C
Air exhaust temp	122.3	C
Exhaust velocity	621.1	FPM
Oil inlet temp	41.8	C
Oil outlet temp	53.6	C
Oil pressure	188.8	kPa
Oil mass flow rate	1.33	LPM
TEG inlet temp	41.3	C
TEG outlet temp	54.3	C
HX Pressure diff	17.3	Pa
Load voltage	23.8885	V
Load current	0.082	A
Load power	2.011	W
Load resistance	291.447	Ω
Desorber OO Temp	42.2	C
Desorber OI Temp	52.8	C

The results from testing these three conditions led to the confirmation of a few relations. First, the author saw an inverse relation between the oil temperature and pressure; as oil inlet and outlet temperature increased, oil pressure decreased. As the air inlet temperature was increased and decreased, by altering the temperature and mass flow rate of the blower, the TEG outlet temperature in a similar fashion. This also led to confirming the relation that an increase in air inlet temperature should result in a greater load power delivered to the TEGs, as TEG power generation is driven by temperature gradients. However, a concerning result from the system tests showed an output load power between 2.011 W – 4.081 W. There were 2 potential system conditions influencing the system. One potential cause was that a significant amount of heat was lost to the environment, while the other cause for low power output was an electrical issue within the TEG. An important note made during testing was that the system was not properly insulated. With this in mind, the author conducted an energy balance to understand where the energy went to in this system.

Chapter 5

HX System Analysis

To better understand the experimental results, the author conducted a detailed energy balance of the HX system was conducted in Appendix C: Complete Calculations for System Energy Balance. This energy balance of the experimental results was crucial to understand why, with a strong heat input from the blower (approximately ranging from 0.7471 – 1.415 kW), there was a low load power delivery (ranging from 2.366 – 4.801 W) to the TEG. An additional step in the author's analysis compared the initial model to the experimental results. This comparison highlighted two experimental issues, the lack of insulation and electrical issues within the programmable load (TEG) itself, which were not accounted for in the initial model.

5.1 Energy Balance

In the TEG/Oil Loop system, there was one heat input source and two to three main outlets for heat to be delivered to. The heat input source was the fan blower, which delivered heat to the HX enclosure and the oil loop, which flowed through the HX enclosure (serving as the cold fluid in the heat exchanger). The channels for the heat to be delivered to were the TEGs within the HX enclosure, the oil within the oil loop, and in the tests with no insulation, heat loss to the surroundings. The energy balance with no insulation was expressed by the following equation:

$$Q_{air} = Q_{TEG} + Q_{oil} + Q_{loss}$$

For each variable, the value was calculated based on the relevant experimental values, and Q_{loss} was determined for the cases without insulation.

Calculation Development [Appendix C]:

The full calculations provide a breakdown of where heat was delivered to and from within the TEG/Oil Loop. The calculations examine the conditions of Table 4-3, maximum temperature and maximum mass flow rate of the fan blower. The Q_{TEG} value was derived by dividing the programmable load's output power by 85%, which was the tested power convertor efficiency.

Variable Definition:

$Q_{air} = Heat\ Input\ from\ Air\ [W]$

$Q_{TEG} = Heat\ delivered\ to\ the\ TEG\ [W]$

$Q_{oil} = Heat\ delivered\ to\ the\ Oil\ [W]$

$Q_{loss} = Heat\ lost\ to\ surroundings\ [W]$

$d_{air} = Inner\ diameter\ of\ the\ fan\ blower\ pipe\ or\ input\ Air\ [m]$

$A_{air} = Area\ of\ the\ fan\ blower\ pipe\ for\ input\ Air\ [m^2]$

$\dot{m}_{air} = Mass\ flow\ rate\ of\ inlet\ air\ [\frac{kg}{s}]$

$c_{p,air} = Specific\ heat\ of\ air\ at\ T_{air,in}\ \left[\frac{kJ}{kg * K}\right]$

$\dot{m}_{oil} = Mass\ flow\ rate\ of\ inlet\ oil\ [\frac{kg}{s}]$

$c_{p,oil} = Specific\ heat\ of\ air\ at\ T_{oil,in}\ \left[\frac{kJ}{kg * K}\right]$

Assumptions:

$d_{air} = 0.0617\ [m]$

$c_{p,air} = 1.042\ [\frac{kJ}{kg * K}]$

$c_{p,oil} = 2.300\ [\frac{kJ}{kg * K}]$

Equations:

$A_{air} = \pi/4 * d_{air}^2$

$\dot{m}_{air} = v_{air} * A_{air} * \rho_{air}$

$\dot{m}_{oil} = \dot{v}_{oil} * \rho_{oil}$

$Q_{air} = \dot{m}_{air} * c_{p,air} * \Delta T_{air}$

$Q_{oil} = \dot{m}_{oil} * c_{p,oil} * \Delta T_{oil}$

$$A_{air} = 0.00299\ m^2$$

$$\dot{m}_{air} = 4.571 \frac{m}{s} * 0.00299\ m^2 * 0.7863 \frac{kg}{m^3} = 0.01075 \frac{kg}{s}$$

$$\dot{m}_{oil} = 0.000024 \frac{m^3}{s} * 862.4 \frac{kg}{m^3} = 0.02070 \frac{kg}{s}$$

$$Q_{air} = 0.01075 \frac{kg}{s} * 1.02 \frac{kJ}{kg * K} * (286.6 - 175.8)\ K = 1.215\ kW$$

$$Q_{oil} = 0.02070 \frac{kg}{s} * 2.0 \frac{kJ}{kg * K} * (68.9 - 52.6)\ K = 0.6748 kW$$

$$Q_{TEG} = \frac{3.505}{85\%} * 10^{-3}(kW) = 4.124 * 10^{-3}\ kW$$

$$Q_{loss} = Q_{air} - Q_{oil} - Q_{TEG} = 0.5360\ kW$$

From the energy balance of the maximum flow rate and maximum temperature condition, as well as the energy balances done in Appendix C for the other two test conditions, it was quite easy to determine the impact a lack of insulation had on the programmable load power output. Lacking insulation resulted in 44.11% of input Q_{air} being lost from the incoming blower air to the surroundings, which significantly affected the amount of heat that could have been channeled to the TEGs and converted into power by the power converter. For the 50% maximum flow rate and maximum temperature condition, 43.56%% of Q_{air} was lost to the environment. Finally, for the 50% maximum flow rate and 50% maximum temperature condition, 41.27% of Q_{air} was lost to the environment. Each scenario resulted in significant heat loss, seemingly unaffected by the input Q_{air}value.

To understand the accuracy of these measurements, an uncertainty propagation of the output parameters was conducted on EES, shown in Appendix C. The uncertainty propagation showed which input parameters influenced the output parameters greatest, and the degree of precision for the results. This also served to understand the potential sources of errors in the experimental values, as the inputs with greater uncertainty drove increased uncertainty in output parameters. The EES output indicated for the Q_{air} outputs, the majority of uncertainty (73.98 – 97.30%) comes from the v_{air} measurements, which were derived from the pressure drop of a Pitot tube in place (with minimal uncertainty due to the change in air temperatures). The uncertainty for v_{air} was determined using the formula $\Delta P = \frac{1}{2} * \rho_{air} * v_{air}^2$ with a known instrument uncertainty of 0.25Pa. Conversely, the majority of uncertainty (96.66 – 98.63%) for Q_{oil} was due to the change in oil temperatures (with minimal uncertainty due to the volume flow rates, which were to the power of 10^{-7}).

There were two potential solutions to minimizing Q_{loss}. The author's belief was that proper insulation for the system, especially at the high-pressure inlet of the HX, and proper resistance within the TEG modules led to very low TEG power outputs would increase TEG power conversion. The system, under proper insulation, would have minimal heat lost to the environment for each condition, resulting in greater power generation by the programmable load (corresponding to the increase in heat transferred to the TEGs within the HX enclosure). Understanding the importance of proper insulation led to the implementation of caulk at the HX inlet, which would seal off potential leaks, and planning additional tests with insulation to determine the programmable loads' power outputs without losing heat to the environment surroundings.

5.2 Experimental and Theoretical Results Comparison

After conducting the experimental tests without insulation, the results were compared with relevant parameters from the initial model shown below.

Table 5-1 Comparison of Theoretical and Experimental Results

	$Q_{air}\ (kW)$	$Q_{oil}\ (kW)$	$Q_{TEG}\ (W)$	$Q_{loss}\ (kW)$
Theoretical Model	1.550	0.756	4.56	0.789
Experimental Results – Condition 1	1.215	0.6748	4.124	0.536
Experimental Results – Condition 2	1.415	0.7935	4.801	0.6164
Experimental Results – Condition 3	0.7471	0.4363	2.366	0.3084

The comparison of these results indicated some key discrepancies in the author's theoretical model and experimental conditions. The experimental Q_{air} values were derived from raw data, while the theoretical Q_{air} value was derived from the thermal resistance network. The assumptions of inlet and outlet air temperatures led to a slightly greater theoretical Q_{air}, calculated through the LMTD approach. When comparing the ratio of $\frac{Q_{oil}}{Q_{air}}$ for each condition to the theoretical model, the ratio of heat transferred to the oil (48.77% of Q_{air}) in the theoretical model was slightly lower than the ratio of each test condition (respectively, 55.54%, 56.07% and 58.40% of Q_{air}).

Intuitively, this led to a decreased power output Q_{TEG} for the experimental conditions, but not to the extent thr data suggested. The experimental Q_{TEG} ranged from 2.366 – 4.801 W, while the theoretical Q_{TEG} "produced" 4.56 W. This led the author and the team to agree that electrical issues with the TEG circuitry were not the main driver of low power conversion. Another key source for the Q_{TEG} discrepancy was the difference between theoretical and experimental values of Q_{loss}, which represented the heat lost to the environment. The amount of heat lost to the environment in the experimental tests led Yue to properly insulate the inlet of the HX enclosure with caulk prior to the next test run. This solution to the low experimental Q_{TEG} values is discussed as future work within the Conclusion.

Chapter 6

Conclusion

This thesis investigated the design and testing of a waste heat absorption facility utilizing a designed HX enclosure, to facilitate heat transfer, and TEGs, to convert input heat into power output. After modeling and manufacturing the HX enclosure through SolidWorks, Shahzaib and Yue assembled the TEG/Oil loop. After the author used the system's thermal resistance network to determine a theoretical Q_{TEG} output, the author and Dr. Rattner ran experiments by varying the input parameters to calculate power outputs Q_{air}, Q_{oil}, and Q_{TEG}. The Q_{TEG} output was minimal (in the range of a few watts) when compared to the input heat Q_{air} (in the range of 0.7471 – 1.415 kW). Conducting energy balances allowed the author to discover significant heat lost to the environment, highlighting a potential flaw in the system. Conducting an analysis of the theoretical and experimental values supported the hypothesis that heat loss to the environment significantly impacted the system's performance.

Further work will focus on evaluating the waste heat absorption facility with caulk implemented at the HX inlet. Tests run after inputting the caulk will properly insulate the system, and the resulting Q values will indicate whether heat lost to the environment is the main driver behind the poor Q_{TEG} output, or there are further electrical issues with the programmable load itself causing low power output. After this analysis, a true TEG/Oil loop recovery system can be tested for optimal TEG performance, without losing significant input heat to the environment.

Appendix A

Complete Calculation for Thermal Resistance Network

The calculations are broken down in terms of "steps" along the thermal resistance network. Each "step" corresponds to a form of resistance encountered within the system (convection, conduction or interface resistance).

Resistance due to Convection, $R_{conv,air}$:

$$Re = \frac{4 * \dot{m}_{air}}{\pi * D_{e,hs} * \mu_{air}}$$

$$Nu_{air} = 0.304 * Re^{0.59} * Pr^{\frac{1}{3}}$$

$$h_{conv} = (Nu_{air} * k_{alum})/(D_{e,hs})$$

$$fin_{lc} = \frac{fin_{base}}{4} + fin_{l}$$

$$A_{fin} = \pi * fin_{base} * fin_{lc}$$

$$fin_{efficiency} = (\frac{\tanh\left(\left(\frac{2 * h_{conv}}{k_{alum} * A_{fin}}\right)^{0.5} * (fin_{lc})^{1.5}\right)}{\left(\frac{2 * h_{conv}}{k_{alum} * A_{fin}}\right)^{0.5} * (fin_{lc})^{1.5}}$$

$$A_{base} = 0.0064\ m^2$$

$$R_{conv,air} = \frac{1}{N * fin_{efficiency} * h_{conv} * A_{base}}$$

Resistance due to Interface 1, $R_{int,1}$: Steel-Steel Interface

$$A_{base} = 0.0064\ m^2$$

$$R_{int,1} = \frac{1}{h_{j,steel-steel} * A_{base}}$$

Resistance due to Conduction, $R_{cond,steel}$:

$$R_{cond,steel} = \frac{L_{plate}}{k_{steel} * A_{base}}$$

Resistance due to Interface 2, $R_{int,2}$: Steel-Steel Interface

$$A_{base} = 0.0064\, m^2$$

$$R_{int,2} = \frac{1}{h_{j,steel-steel} * A_{base}}$$

Resistance due to TEG, R_{TEG}:

$$R_{TEG} = 0.667 \frac{K}{W}$$

Resistance due to Interface 3, $R_{int,3}$: Aluminum-Steel Interface

$$A_{base} = 0.0064\, m^2$$

$$R_{int,3} = \frac{1}{h_{j,alum-steel} * A_{base}}$$

Resistance due to Conduction, $R_{cond,cp}$:

$$R_{cond,cp} = \frac{L_{cp}}{k_{alum} * A_{base}}$$

Resistance due to Interface 4, $R_{int,4}$: Aluminum-Aluminum Interface

$$A_{base} = 0.0064\, m^2$$

$$R_{int,4} = \frac{1}{h_{j,alum-alum} * A_{base}}$$

Resistance due to Convection, $R_{conv,wb}$:

$$Re_{wb} = \frac{4 * \dot{m}_{oil}}{\pi * D_{wb} * \mu_{oil}}$$

$$Nu_{oil} = 0.023 * Re^{0.80} * Pr^{0.4}$$

$$h_{conv,wb} = (Nu_{oil} * k_{oil})/(D_{wb})$$

$$fin_{wb,lc} = \frac{fin_{wb,t}}{2} + fin_{wb,l}$$

$$A_{fin,wb} = \pi * fin_{wb,t} * fin_{wb,l}$$

$$fin_{efficiency,wb} = (\frac{\tanh\left(\left(\frac{2 * h_{conv,wb}}{k_{oil} * A_{fin,wb}}\right)^{0.5} * \left(fin_{wb,lc}\right)^{1.5}\right)}{\left(\frac{2 * h_{conv,wb}}{k_{oil} * A_{fin,wb}}\right)^{0.5} * \left(fin_{wb,lc}\right)^{1.5}}$$

$$A_{base} = 0.0064\ m^2$$

$$R_{conv,wb} = \frac{1}{N * fin_{efficiency,wb} * h_{conv,wb} * A_{base}}$$

Calculations:

Resistance due to Convection, $R_{conv,air}$:

$$Re = \frac{4 * 0.073(\frac{kg}{s})}{\pi * (0.08m) * (3.616 * 10^{-5}) \frac{(N * s)}{m^2}} = 32{,}135$$

$$Nu_{air} = 0.304 * 32135^{0.59} * 0.689^{\frac{1}{3}} = 122.5$$

$$h_{conv} = \frac{\left(122.5 * 4.679 * 10^{-4} \left(\frac{W}{m * K}\right)\right)}{0.08m} = 0.8694\ (\frac{W}{m^2 * K})$$

$$fin_{lc} = \frac{0.0033}{4} + 0.033 = 0.03383\ m$$

$$A_{fin} = \pi * 0.0033m * 0.03383m = 0.0003507\ m^2$$

$$fin_{efficiency} = \left(\frac{\tanh\left(\left(\frac{2 * 0.8694 \left(\frac{W}{m^2 * K}\right)}{4.679 * 10^{-4} \left(\frac{W}{m * K}\right) * 0.0003507\ m^2} \right)^{0.5} * (0.03383\ m)^{1.5} \right)}{\left(\frac{2 * 0.8694 \left(\frac{W}{m^2 * K}\right)}{4.679 * 10^{-4} \left(\frac{W}{m * K}\right) * 0.0003507\ m^2} \right)^{0.5} * (0.03383\ m)^{1.5}} \right) = 0.9997$$

$$A_{base} = 0.0064\ m^2$$

$$R_{conv,air} = \frac{1}{256 * 0.9997 * 0.8694 \left(\frac{W}{m^2 * K}\right) * 0.0064\ m^2} = 0.7022 \frac{K}{W}$$

Resistance due to Interface 1, $R_{int,1}$: Steel-Steel Interface

$$A_{base} = 0.0064\ m^2$$

$$R_{int,1} = \frac{1}{4000\ (\frac{W}{m^2 * K}) * 0.0064 m^2} = 0.039 \frac{K}{W}$$

Resistance due to Conduction, $R_{cond,steel}$:

$$R_{cond,steel} = \frac{0.003175m}{25(\frac{W}{m * K}) * 0.0064 m^2} = 0.020 \frac{K}{W}$$

Resistance due to Interface 2, $R_{int,2}$: Steel-Steel Interface

$$A_{base} = 0.0064\ m^2$$

$$R_{int,2} = \frac{1}{4000\ (\frac{W}{m^2 * K}) * 0.0064 m^2} = 0.039 \frac{K}{W}$$

Resistance due to TEG, R_{TEG}:

$$R_{TEG} = 0.667 \frac{K}{W}$$

Resistance due to Interface 3, $R_{int,3}$: Aluminum-Steel Interface

$$A_{base} = 0.0064\ m^2$$

$$R_{int,3} = \frac{1}{4500\ (\frac{W}{m^2 * K}) * 0.0064 m^2} = 0.034 \frac{K}{W}$$

Resistance due to Conduction, $R_{cond,cp}$:

$$R_{cond,cp} = \frac{0.003m}{237\ (\frac{W}{m * K}) * 0.0064 m^2} = 0.002 \frac{K}{W}$$

Resistance due to Interface 4, $R_{int,4}$: Aluminum-Aluminum Interface

$$A_{base} = 0.0064\ m^2$$

$$R_{int,4} = \frac{1}{12000\ (\frac{W}{m^2 * K}) * 0.0064 m^2} = 0.013 \frac{K}{W}$$

Resistance due to Convection, $R_{conv,wb}$:

$$Re_{wb} = \frac{4 * 0.02618(\frac{kg}{s})}{\pi * (0.065m) * (0.0022) \frac{(N * s)}{m^2}} = 233.1$$

$$Nu_{oil} = 0.023 * 233.1^{0.80} * 51.11^{0.4} = 8.693$$

$$h_{conv,wb} = \frac{8.693 * 0.099 \left(\frac{W}{m * K}\right)}{0.065m} = 13.24 \frac{W}{m^2 * K}$$

$$fin_{wb,lc} = \frac{0.000127}{2} m + 0.009144m = 0.009208\ m$$

$$A_{fin,wb} = \pi * 0.000127m * 0.009144 = 0.000001161\ m^2$$

$$fin_{efficiency,wb} = \left(\frac{\tanh\left(\left(\frac{2 * 13.24 \left(\frac{W}{m^2 * K}\right)}{0.099 \left(\frac{W}{m * K}\right) * 0.000001161\, m^2} \right)^{0.5} * (0.009208\, m)^{1.5} \right)}{\left(\frac{2 * 13.24 \left(\frac{W}{m^2 * K}\right)}{0.099 \left(\frac{W}{m * K}\right) * 0.000001161\, m^2} \right)^{0.5} * (0.009208\, m)^{1.5}} \right) = 0.07458$$

$$A_{base} = 0.0064\, m^2$$

$$R_{conv,wb} = \frac{1}{12 * 0.07458 * 13.24 \left(\frac{W}{m^2 * K}\right) * 0.0064\, m^2} = 13.19 \frac{K}{W}$$

$$R_{TOT} = R_{conv,air} + R_{int,1} + R_{cond,steel} + R_{int,3} + R_{TEG} + R_{int,3} + R_{cond,cp} + R_{int,4} + R_{conv,wb}$$

$$= \mathbf{14.62} \frac{\boldsymbol{K}}{\boldsymbol{W}}$$

The R_{TOT} value calculated is the thermal resistance through one TEG; so, UA, the overall resistance, was calculated by $1/UA = (1/R_{TOT}+1/R_{TOT}+1/R_{TOT}+1/R_{TOT}+1/R_{TOT}+1/R_{TOT})$.

Appendix B

Complete Calculations for Initial Model

The Initial Model was setup and calculated via Engineering Equation Solver (EES). The code for this program is attached in Appendix B.

```
"!Known System Properties"

T_air_in = 793 [K]                                          "Temperature of air in"
T_oil_in = 393 [K]                                          "Temperature of oil in"
mdot_air = 0.073 [kg/s]                                     "mass flow rate of air"
mdot_oil = 0.02618 [kg/s]                                   "mass flow rate of oil"
cp_air = 1.098 [kJ/kg-K]                                    "specific heat of air at T = 793K"
cp_oil = cp(Paratherm_NF, T=52.6 [C])                       "specific heat of air at T = 393K"
h1_air = 811.0 [kJ/kg]                                      "specific enthalpy of air at T_air_in"
h1_oil = enthalpy(Paratherm_NF, T=120 [C], P=101.325 [kPa]) "specific enthalpy of oil at T_oil_in"

k_alum = 5.679E-4 [W/m-k]                                   "thermal conductivity of aluminum heat sink at T_air_in"
k_wb = conductivity(Paratherm_NF, T=120 [C])                "thermal conductivity of steel water block"
```

Figure B-1 Known system inputs for HX system's theoretical model.

The values in B-1 were known/assumed system properties to run the model and to determine power output Q. A built-in EES function was used to find the properties of the oil, Paratherm NF. The values in B-2 were used to calculate the convection coefficients which were used in determining the overall system resistance UA.

```
"!System Resistance"

R_conv = 1/(N*fin_efficiency*h_conv*A_base)                  "convection resistance through heat sinks"
R_int_1 = 0.039 [K/W]                                        "resistance through first interface"
R_cond_plate = 0.020 [K/W]                                   "conduction resistance through steel plate"
R_int_2 = 0.039 [K/W]                                        "resistance through second interface"
R_TEG = 0.667 [K/W]                                          "conduction resistance through TEG module"
R_int_3 = 0.034 [K/W]                                        "resistance through third interface"
R_cond_cp = 0.002 [K/W]                                      "conduction resistance through coupling plate"
R_int_4 = 0.013 [K/W]                                        "resistance through fourth interface"
R_conv_wb = 1/(N_wb*fin_efficiency_wb*h_conv_wb*A_base_wb)   "convection resistance through water block"

R_TOT =(R_conv+R_int_1+R_cond_plate+R_int_2+R_TEG+R_int_3+R_cond_cp+R_int_4+R_conv_wb)   "resistance through one heat sink series"
UA = (1/R_TOT)                                               "overall system resistance"
```

Figure B-2 Overall system resistance calculations.

Calculations:

$$Q_{air} = UA * LMTD$$

$$LMTD = \frac{\left(T_{air,in} - T_{oil,out}\right) - \left(T_{air,out} - T_{oil,out}\right)}{ln\left(\frac{\left(T_{air,in} - T_{oil,out}\right)}{\left(T_{air,out} - T_{oil,out}\right)}\right)}$$

$$h_{2,air} = \frac{Q}{\dot{m}_{air} * c_{p,air}} + h_{1,air}$$

$$h_{2,oil} = \frac{Q}{\dot{m}_{oil} * c_{p,oil}} + h_{1,oil}$$

$$T_{air,out} = \frac{h_{2,air} - h_{1,air}}{c_{p,air}} + T_{air,in}$$

$$T_{oil,out} = \frac{h_{2,oil} - h_{1,oil}}{c_{p,oil}} + T_{oil,in}$$

$$Q_{oil} = \dot{m}_{oil} * c_{p,oil} * \Delta T_{oil}$$

The above equations were solved for simultaneously using EES, resulting in:

$$\boldsymbol{Q_{air} = 1.550\ kW}$$

$$\boldsymbol{LMTD = 89.86\ K}$$

$$\boldsymbol{h_{2,air} = 852.8 \frac{kJ}{kg}}$$

$$\boldsymbol{h_{2,oil} = 916.8 \frac{kJ}{kg}}$$

$$\boldsymbol{T_{air,out} = 691.1\ K}$$

$$\boldsymbol{T_{oil,out} = 420.8\ K}$$

$$\boldsymbol{Q_{oil} = 0.756\ kW}$$

Appendix C

Complete Calculations for System Energy Balance

Equations:

$$Q_{IN} = Q_{OUT} \rightarrow Q_{air} = Q_{oil} + Q_{TEG} + Q_{LOSS}$$

$$A_{air} = \pi/4 * d_{air}^2$$

$$\dot{m}_{air} = v_{air} * A_{air} * \rho_{air}$$

$$\dot{m}_{oil} = \dot{v}_{oil} * \rho_{oil}$$

$$Q_{air} = \dot{m}_{air} * c_{p,air} * \Delta T_{air}$$

$$Q_{oil} = \dot{m}_{oil} * c_{p,oil} * \Delta T_{oil}$$

$$Q_{TEG} = \frac{Load_{Power}}{85\%}$$

$$Q_{LOSS} = Q_{air} - Q_{oil} - Q_{TEG}$$

Calculations: $A_{air} = 0.00299\ m^2$

For Maximum Flow Rate and Maximum Temperature Blower Conditions:

$$\dot{m}_{air} = 4.571 \frac{m}{s} * 0.00299\ m^2 * 0.7863 \frac{kg}{m^3} = 0.01075 \frac{kg}{s}$$

$$\dot{m}_{oil} = 0.000024 \frac{m^3}{s} * 862.4 \frac{kg}{m^3} = 0.02070 \frac{kg}{s}$$

$$Q_{air} = 0.01075 \frac{kg}{s} * 1.02 \frac{kJ}{kg * K} * (286.6 - 175.8)\ K = 1.215\ kW$$

$$Q_{oil} = 0.02070 \frac{kg}{s} * 2.000 \frac{kJ}{kg * K} * (68.9 - 52.6)\ K = 0.6748 kW$$

$$Q_{TEG} = \frac{3.505}{85\%} * 10^{-3}(kW) = 4.124 * 10^{-3}\ kW$$

$$Q_{loss} = Q_{air} - Q_{oil} - Q_{TEG} = 0.5360\ kW$$

For 50% Maximum Flow Rate and Maximum Temperature Blower Conditions:

$$\dot{m}_{air} = 3.2258\frac{m}{s} * 0.00299\ m^2 * .7577\frac{kg}{m^3} = 0.00731\frac{kg}{s}$$

$$\dot{m}_{oil} = 0.00002483\frac{m^3}{s} * 859.1\frac{kg}{m^3} = 0.02133\frac{kg}{s}$$

$$Q_{air} = 0.00731\frac{kg}{s} * 1.023\frac{kJ}{kg * K} * (381.9 - 192.7)\ K = 1.415\ kW$$

$$Q_{oil} = 0.02133\frac{kg}{s} * 2.000\frac{kJ}{kg * K} * (76.8 - 58.2)\ K = 0.7935\ kW$$

$$Q_{TEG} = \frac{4.081}{85\%} * 10^{-3}(kW) = 4.801 * 10^{-3}\ kW$$

$$Q_{loss} = Q_{air} - Q_{oil} - Q_{TEG} = 0.6164\ kW$$

For 50% Maximum Flow Rate and 50% Maximum Temperature Blower Conditions:

$$\dot{m}_{air} = 3.1552\frac{m}{s} * 0.00299\ m^2 * .0.8926\frac{kg}{m^3} = 0.00842\frac{kg}{s}$$

$$\dot{m}_{oil} = 0.00002217\frac{m^3}{s} * 869.7\frac{kg}{m^3} = 0.01928\frac{kg}{s}$$

$$Q_{air} = 0.00842\frac{kg}{s} * 1.013\frac{kJ}{kg * K} * (209.9 - 122.3)\ K = 0.7471\ kW$$

$$Q_{oil} = 0.01928\frac{kg}{s} * 1.918\frac{kJ}{kg * K} * (53.6 - 41.8)\ K = 0.4363kW$$

$$Q_{TEG} = \frac{2.011}{85\%} * 10^{-3}(kW) = 2.366 * 10^{-3}\ kW$$

$$Q_{loss} = Q_{air} - Q_{oil} - Q_{TEG} = 0.3084\ kW$$

Another important metric to measure was the Uncertainty Propagation. This allowed the author to understand which input parameters were most influencing the output Q values, for both air and oil. Understanding the uncertainty of the data allowed the author to determine the quality and level of precision for the output parameters.

Unit Settings: SI C kPa kJ mass deg

Variable±Uncertainty	Partial derivative	% of uncertainty
Q_{air1} = 1.215±0.02149 [kW]		
$\delta_{T,air1}$ = 110.8±1 [K]	$\partial Q_{air1}/\partial \delta_{T,air1}$ = 0.01096	26.02 %
$\delta_{T,air2}$ = 189.2±1 [K]	$\partial Q_{air1}/\partial \delta_{T,air2}$ = 0	0.00 %
$\delta_{T,air3}$ = 87.6±1 [K]	$\partial Q_{air1}/\partial \delta_{T,air3}$ = 0	0.00 %
$\delta_{T,oil1}$ = 16.3±1 [K]	$\partial Q_{air1}/\partial \delta_{T,oil1}$ = 0	0.00 %
$\delta_{T,oil2}$ = 18.6±1 [K]	$\partial Q_{air1}/\partial \delta_{T,oil2}$ = 0	0.00 %
$\delta_{T,oil3}$ = 11.8±1 [K]	$\partial Q_{air1}/\partial \delta_{T,oil3}$ = 0	0.00 %
v_{air1} = 4.571±0.06956 [m/s]	$\partial Q_{air1}/\partial v_{air1}$ = 0.2658	73.98 %
v_{air2} = 3.226±0.1023 [m/s]	$\partial Q_{air1}/\partial v_{air2}$ = 0	0.00 %
v_{air3} = 3.155±0.08878 [m/s]	$\partial Q_{air1}/\partial v_{air3}$ = 0	0.00 %
$vdot_{oil1}$ = 0.000024±2.400E-07 [m^3/s]	$\partial Q_{air1}/\partial vdot_{oil1}$ = 0	0.00 %
$vdot_{oil2}$ = 0.00002483±2.483E-07 [m^3/s]	$\partial Q_{air1}/\partial vdot_{oil2}$ = 0	0.00 %
$vdot_{oil3}$ = 0.00002217±2.217E-07 [m^3/s]	$\partial Q_{air1}/\partial vdot_{oil3}$ = 0	0.00 %
Q_{air2} = 1.415±0.04547 [kW]		
$\delta_{T,air1}$ = 110.8±1 [K]	$\partial Q_{air2}/\partial \delta_{T,air1}$ = 0	0.00 %
$\delta_{T,air2}$ = 189.2±1 [K]	$\partial Q_{air2}/\partial \delta_{T,air2}$ = 0.007478	2.70 %
$\delta_{T,air3}$ = 87.6±1 [K]	$\partial Q_{air2}/\partial \delta_{T,air3}$ = 0	0.00 %
$\delta_{T,oil1}$ = 16.3±1 [K]	$\partial Q_{air2}/\partial \delta_{T,oil1}$ = 0	0.00 %
$\delta_{T,oil2}$ = 18.6±1 [K]	$\partial Q_{air2}/\partial \delta_{T,oil2}$ = 0	0.00 %
$\delta_{T,oil3}$ = 11.8±1 [K]	$\partial Q_{air2}/\partial \delta_{T,oil3}$ = 0	0.00 %
v_{air1} = 4.571±0.06956 [m/s]	$\partial Q_{air2}/\partial v_{air1}$ = 0	0.00 %
v_{air2} = 3.226±0.1023 [m/s]	$\partial Q_{air2}/\partial v_{air2}$ = 0.4386	97.30 %
v_{air3} = 3.155±0.08878 [m/s]	$\partial Q_{air2}/\partial v_{air3}$ = 0	0.00 %
$vdot_{oil1}$ = 0.000024±2.400E-07 [m^3/s]	$\partial Q_{air2}/\partial vdot_{oil1}$ = 0	0.00 %
$vdot_{oil2}$ = 0.00002483±2.483E-07 [m^3/s]	$\partial Q_{air2}/\partial vdot_{oil2}$ = 0	0.00 %
$vdot_{oil3}$ = 0.00002217±2.217E-07 [m^3/s]	$\partial Q_{air2}/\partial vdot_{oil3}$ = 0	0.00 %

Figure C-1 Uncertainty Propagation of Q_{air} at the first and second test conditions.

Q_{air3} = 0.7471±0.02269 [kW]		
$\delta_{T,air1}$ = 110.8±1 [K]	$\partial Q_{air3}/\partial \delta_{T,air1}$ = 0	0.00 %
$\delta_{T,air2}$ = 189.2±1 [K]	$\partial Q_{air3}/\partial \delta_{T,air2}$ = 0	0.00 %
$\delta_{T,air3}$ = 87.6±1 [K]	$\partial Q_{air3}/\partial \delta_{T,air3}$ = 0.008529	14.13 %
$\delta_{T,oil1}$ = 16.3±1 [K]	$\partial Q_{air3}/\partial \delta_{T,oil1}$ = 0	0.00 %
$\delta_{T,oil2}$ = 18.6±1 [K]	$\partial Q_{air3}/\partial \delta_{T,oil2}$ = 0	0.00 %
$\delta_{T,oil3}$ = 11.8±1 [K]	$\partial Q_{air3}/\partial \delta_{T,oil3}$ = 0	0.00 %
v_{air1} = 4.571±0.06956 [m/s]	$\partial Q_{air3}/\partial v_{air1}$ = 0	0.00 %
v_{air2} = 3.226±0.1023 [m/s]	$\partial Q_{air3}/\partial v_{air2}$ = 0	0.00 %
v_{air3} = 3.155±0.08878 [m/s]	$\partial Q_{air3}/\partial v_{air3}$ = 0.2368	85.87 %
$vdot_{oil1}$ = 0.000024±2.400E-07 [m^3/s]	$\partial Q_{air3}/\partial vdot_{oil1}$ = 0	0.00 %
$vdot_{oil2}$ = 0.00002483±2.483E-07 [m^3/s]	$\partial Q_{air3}/\partial vdot_{oil2}$ = 0	0.00 %
$vdot_{oil3}$ = 0.00002217±2.217E-07 [m^3/s]	$\partial Q_{air3}/\partial vdot_{oil3}$ = 0	0.00 %
Q_{oil1} = 0.6748±0.04194 [kW]		
$\delta_{T,air1}$ = 110.8±1 [K]	$\partial Q_{oil1}/\partial \delta_{T,air1}$ = 0	0.00 %
$\delta_{T,air2}$ = 189.2±1 [K]	$\partial Q_{oil1}/\partial \delta_{T,air2}$ = 0	0.00 %
$\delta_{T,air3}$ = 87.6±1 [K]	$\partial Q_{oil1}/\partial \delta_{T,air3}$ = 0	0.00 %
$\delta_{T,oil1}$ = 16.3±1 [K]	$\partial Q_{oil1}/\partial \delta_{T,oil1}$ = 0.0414	97.41 %
$\delta_{T,oil2}$ = 18.6±1 [K]	$\partial Q_{oil1}/\partial \delta_{T,oil2}$ = 0	0.00 %
$\delta_{T,oil3}$ = 11.8±1 [K]	$\partial Q_{oil1}/\partial \delta_{T,oil3}$ = 0	0.00 %
v_{air1} = 4.571±0.06956 [m/s]	$\partial Q_{oil1}/\partial v_{air1}$ = 0	0.00 %
v_{air2} = 3.226±0.1023 [m/s]	$\partial Q_{oil1}/\partial v_{air2}$ = 0	0.00 %
v_{air3} = 3.155±0.08878 [m/s]	$\partial Q_{oil1}/\partial v_{air3}$ = 0	0.00 %
$vdot_{oil1}$ = 0.000024±2.400E-07 [m^3/s]	$\partial Q_{oil1}/\partial vdot_{oil1}$ = 28116	2.59 %
$vdot_{oil2}$ = 0.00002483±2.483E-07 [m^3/s]	$\partial Q_{oil1}/\partial vdot_{oil2}$ = 0	0.00 %
$vdot_{oil3}$ = 0.00002217±2.217E-07 [m^3/s]	$\partial Q_{oil1}/\partial vdot_{oil3}$ = 0	0.00 %

Figure C-2 Uncertainty Propagation of at Q_{air} the third test condition and Q_{oil} at the first test condition.

Q_{oil2} = 0.7935±0.04339 [kW]		
$\delta_{T,air1}$ = 110.8±1 [K]	$\partial Q_{oil2}/\partial \delta_{T,air1}$ = 0	0.00 %
$\delta_{T,air2}$ = 189.2±1 [K]	$\partial Q_{oil2}/\partial \delta_{T,air2}$ = 0	0.00 %
$\delta_{T,air3}$ = 87.6±1 [K]	$\partial Q_{oil2}/\partial \delta_{T,air3}$ = 0	0.00 %
$\delta_{T,oil1}$ = 16.3±1 [K]	$\partial Q_{oil2}/\partial \delta_{T,oil1}$ = 0	0.00 %
$\delta_{T,oil2}$ = 18.6±1 [K]	$\partial Q_{oil2}/\partial \delta_{T,oil2}$ = 0.04266	96.66 %
$\delta_{T,oil3}$ = 11.8±1 [K]	$\partial Q_{oil2}/\partial \delta_{T,oil3}$ = 0	0.00 %
v_{air1} = 4.571±0.06956 [m/s]	$\partial Q_{oil2}/\partial v_{air1}$ = 0	0.00 %
v_{air2} = 3.226±0.1023 [m/s]	$\partial Q_{oil2}/\partial v_{air2}$ = 0	0.00 %
v_{air3} = 3.155±0.08878 [m/s]	$\partial Q_{oil2}/\partial v_{air3}$ = 0	0.00 %
$vdot_{oil1}$ = 0.000024±2.400E-07 [m^3/s]	$\partial Q_{oil2}/\partial vdot_{oil1}$ = 0	0.00 %
$vdot_{oil2}$ = 0.00002483±2.483E-07 [m^3/s]	$\partial Q_{oil2}/\partial vdot_{oil2}$ = 31958	3.34 %
$vdot_{oil3}$ = 0.00002217±2.217E-07 [m^3/s]	$\partial Q_{oil2}/\partial vdot_{oil3}$ = 0	0.00 %
Q_{oil3} = 0.4363±0.03723 [kW]		
$\delta_{T,air1}$ = 110.8±1 [K]	$\partial Q_{oil3}/\partial \delta_{T,air1}$ = 0	0.00 %
$\delta_{T,air2}$ = 189.2±1 [K]	$\partial Q_{oil3}/\partial \delta_{T,air2}$ = 0	0.00 %
$\delta_{T,air3}$ = 87.6±1 [K]	$\partial Q_{oil3}/\partial \delta_{T,air3}$ = 0	0.00 %
$\delta_{T,oil1}$ = 16.3±1 [K]	$\partial Q_{oil3}/\partial \delta_{T,oil1}$ = 0	0.00 %
$\delta_{T,oil2}$ = 18.6±1 [K]	$\partial Q_{oil3}/\partial \delta_{T,oil2}$ = 0	0.00 %
$\delta_{T,oil3}$ = 11.8±1 [K]	$\partial Q_{oil3}/\partial \delta_{T,oil3}$ = 0.03698	98.63 %
v_{air1} = 4.571±0.06956 [m/s]	$\partial Q_{oil3}/\partial v_{air1}$ = 0	0.00 %
v_{air2} = 3.226±0.1023 [m/s]	$\partial Q_{oil3}/\partial v_{air2}$ = 0	0.00 %
v_{air3} = 3.155±0.08878 [m/s]	$\partial Q_{oil3}/\partial v_{air3}$ = 0	0.00 %
$vdot_{oil1}$ = 0.000024±2.400E-07 [m^3/s]	$\partial Q_{oil3}/\partial vdot_{oil1}$ = 0	0.00 %
$vdot_{oil2}$ = 0.00002483±2.483E-07 [m^3/s]	$\partial Q_{oil3}/\partial vdot_{oil2}$ = 0	0.00 %
$vdot_{oil3}$ = 0.00002217±2.217E-07 [m^3/s]	$\partial Q_{oil3}/\partial vdot_{oil3}$ = 19684	1.37 %

Figure C-3 Uncertainty Propagation of at the second and third test conditions.

BIBLIOGRAPHY

1] G. Singh, “Advanced Combustion Engines,” *Department of Energy,* 2014. [Online]. Available: https://energy.gov/eere/vehicles/advanced-combustion-engines.

[2] J. Fairbanks, “Automotive Thermoelectric Generators and HVAC,” Energy *Efficiency & Renewable Energy,* 17-May-2013. [Online]. Available: https://energy.gov/sites/prod/files/2014/03/f13/ace00e_fairbanks_2013_o.pdf

[3] C.-C. Weng and M.-J. Huang, “A simulation study of automotive waste heat recovery using a thermoelectric power generator,” *International Journal of Thermal Sciences,* vol. 71, pp. 302–309, Sep. 2013.

[4] “Brief History of Thermoelectrics,” *History of Thermoelectrics.* [Online]. Available: http://www.thermoelectrics.caltech.edu/thermoelectrics/history.html.

[5] B. Orr, A. Akbarzadeh, M. Mochizuki, and R. Singh, “A review of car waste heat recovery systems utilising thermoelectric generators and heat pipes,” *Applied Thermal Engineering,* vol. 101, pp. 490–495, May 2016.

[6] T.-M. Jeng, S.-C. Tzeng, B.-J. Yang, and Y.-C. Li, “Design, Manufacture and Performance Test of the Thermoelectric Generator System for Waste Heat Recovery of Engine Exhaust,” *Inventions,* vol. 1, no. 1, p. 2, Nov. 2016.

[7] L. L. Baranowski, G. J. Snyder, and E. S. Toberer, “Effective thermal conductivity in thermoelectric materials,” *Journal of Applied Physics,* vol. 113, no. 20, pp. 204–214, May 2013.

[8] R. Romero-Méndez, M. Sen, K. Yang, and R. Mcclain, “Effect of fin spacing on convection in a plate fin and tube heat exchanger,” *International Journal of Heat and Mass Transfer,* vol. 43, no. 1, pp. 39–51, 2000.

[9] T. L. Bergman, A. S. Lavine, F. P. Incropera, and D. P. DeWitt, *Fundamentals of Heat and Mass Transfer*. Hoboken, NJ: Wiley, 2011.

[10] B. Yazicioğlu and H. Yüncü, “Optimum fin spacing of rectangular fins on a vertical base in free convection heat transfer,” *SpringerLink,* 06-Dec-2006. [Online]. Available: https://link.springer.com/article/10.1007/s00231-006-0207-6.

[11] J.-cheng Liu, S.-you Zhang, X.-yue Zhao, G.-dong Yi, and Z.-yong Zhou, “Influence of fin arrangement on fluid flow and heat transfer in the inlet of a plate-fin heat exchanger,”

SpringerLink, 01-Oct-2015. [Online]. Available: https://link.springer.com/article/10.1631%2Fjzus.A1400270.

[12] G. P. Meisner, "Thermoelectric Generator Development for Automotive Waste ...," *Advanced Thermoelectric Materials and Generator Technology for Automotive Waste Heat at GM*, 03-Jan-2011. [Online]. Available: http://www.bing.com/cr?IG=74F026745C76408EB519EEF6E4459A71&CID=0410362D17C360B1080F3D1716C5616B&rd=1&h=zfV2QnKC0xkYqLBkE2hLi4ChtGsAkQosBAJWV1-BmWI&v=1&r=http%3a%2f%2fenergy.gov%2fsites%2fprod%2ffiles%2f2014%2f03%2ff8%2fdeer10_meisner.pdf&p=DevEx,5065.1.

[13] A. M. Mira, "The Design, Testing, and Manufacturing of a Pin Fin ...," *Digital Commons @ Cal Poly*, Mar-2013. [Online]. Available: http://www.bing.com/cr?IG=FF8AB76B990C449F9D59114B1FFED120&CID=093E8C63F5CE665018398750F4C8675D&rd=1&h=zo0nGx9C365YVEUGLUdTVB1Q6N_RJ1hMWDSFi_9arUc&v=1&r=http%3a%2f%2fdigitalcommons.calpoly.edu%2fcgi%2fviewcontent.cgi%3farticle%3d1135%26context%3dimesp&p=DevEx,5068.1.

[14] J. A. Ward, "MEAN TEMPERATURE DIFFERENCE," *A-to-Z Guide to Thermodynamics, Heat and Mass Transfer, and Fluids Engineering*, 14-Feb-2011. [Online]. Available: http://www.thermopedia.com/content/945/.

ACADEMIC VITA

Shiven Patel

shivenpatel112@gmail.com

EDUCATION

The Pennsylvania State University — **University Park, PA**
Schreyer Honors College — Expected Dec. 2017
B.S. Mechanical Engineering

PROFESSIONAL EXPERIENCE

Williams Companies — **Tulsa, OK**
Asset Integrity Intern — May. 2017 – Aug. 2017

- Provide technical guidance to Operations by performing crack categorization for 18 pipeline segments, spanning 800+ miles, to proactively prevent pipeline leakage and ruptures
- Perform statistical analysis on pipeline lab test data worth over $4MM, using PowerBI, to identify pipeline sample test failure trends and report trends to senior leadership
- Create new Welding team and develop team Charter to present to VP of Safety & Operational Discipline

Kimberly Clark Corporation — **Neenah, WI**
Engineering Co-op – KimTech Plant — Aug. 2016 – Dec. 2016

- Created schematics of compressed air pipelines of the manufacturing floor through AutoCAD, in order to minimize excess airflow to machines, reducing annual HVAC costs by up to $70,000
- Designed SolidWorks models, utilizing DFM principles, for Design team to deliver 7 high quality prototypes to K-C Product Development teams

Danaher Corporation — **Fort Collins, CO**
BOLD Intern – Hach Facility — May 2016 – Aug. 2016

- Initiated and drove Process Improvement in a pick-and-pack cell to enhance Productivity and Quality Key Performance Indicators (KPIs), by 52% and 100%, respectively
- Organized and executed Kaizen event to improve material flow and in-line quality checks of cell, collaborating with area managers and cell operators, leading to $146,000 in total cost savings
- Ensured sustainment by motivating operators to utilize Lean tools such as Standard Work, 5S, One-Piece Flow and Visual Daily Management, to maintain newly established KPIs

LEADERSHIP EXPERIENCE

The Schreyer Consulting Group — **University Park, PA**
Project Chair — Dec. 2014 – May 2015

- Connected with a College of Agriculture Professor and collaborated on an Ag-Tech industry white paper to bridge the knowledge gaps between investors in Ag-Tech and Penn State Ag Professors
- Headed committee to acquire consulting projects with professors and local businesses to improve the business of clients by executing customized business solutions

Delta Kappa Epsilon Fraternity — **University Park, PA**
House Manager — Dec. 2014 – May 2015

- Instituted a ten-member housing committee responsible for keeping a house of 38 people functioning through house maintenance and improvement subcommittees with a $40,000 budget
- Coordinated with Exec board, professional companies, and landlord to address housing issues

VOLUNTEER

Shree Swaminarayan Temple — **Secaucus, NJ**
Maintenance Committee Leader — Jan. 2007 – Aug. 2014

- Dedicated over 500 hours to numerous temple quality improvement efforts, including establishing a Maintenance committee to oversee and further improve condition of the temple

SKILLS

Technical: Experienced in SolidWorks, MS Excel, PowerPoint, MS PowerBI, AutoCAD, Lean Manufacturing Principles